



LAWRENCE
LIVERMORE
NATIONAL
LABORATORY

PARA-H₂ TO ORTHO-H₂ CONVERSION IN A FULL-SCALE AUTOMOTIVE CRYOGENIC PRESSURIZED HYDROGEN STORAGE UP TO 345 BAR

G. Petitpas, S. M. Aceves, M. J. Matthews, J. R.
Smith

November 22, 2013

International Journal of Hydrogen Energy

Disclaimer

This document was prepared as an account of work sponsored by an agency of the United States government. Neither the United States government nor Lawrence Livermore National Security, LLC, nor any of their employees makes any warranty, expressed or implied, or assumes any legal liability or responsibility for the accuracy, completeness, or usefulness of any information, apparatus, product, or process disclosed, or represents that its use would not infringe privately owned rights. Reference herein to any specific commercial product, process, or service by trade name, trademark, manufacturer, or otherwise does not necessarily constitute or imply its endorsement, recommendation, or favoring by the United States government or Lawrence Livermore National Security, LLC. The views and opinions of authors expressed herein do not necessarily state or reflect those of the United States government or Lawrence Livermore National Security, LLC, and shall not be used for advertising or product endorsement purposes.

PARA-H₂ TO ORTHO-H₂ CONVERSION IN A FULL-SCALE AUTOMOTIVE CRYOGENIC PRESSURIZED HYDROGEN STORAGE UP TO 345 BAR

Guillaume Petitpas, Salvador M. Aceves,
Manyalibo J. Matthews, James R. Smith

Lawrence Livermore National Laboratory
7000 East Avenue, Livermore, CA, USA

Abstract

We have examined heat absorption from the transition between the two quantum states of the hydrogen molecule (para-ortho) in a full-scale (151 L internal volume) automotive cryogenic pressure vessel at pressures and temperatures up to 345 bar and 300 K, and densities between 14 and 67 g/L (2.1-10.1 kgH₂). The relative concentration of the two species is measured using rotational Raman scattering and verified by calorimetry. In fifteen experiments spanning a full year, we repeatedly filled the vessel with saturated LH₂ at near ambient pressure (2-3 bar), very low temperatures (20.3-25 K), varying densities, and very high para-H₂ fraction (99.7%). We subsequently monitored vessel pressure and temperature while performing periodic ortho-H₂ concentration measurements with rotational Raman scattering as the vessel warmed up and pressurized due to environmental heat entry.

Experiments show that para-ortho H₂ conversion typically becomes active after 10-15 days of dormancy (“initiation” stage), when H₂ temperature reaches 70-80 K. Para-ortho H₂ conversion then approaches completion (equilibrium) in 25-30 days when the vessel reaches 100-120 K at ~50 g/L density. Warmer temperatures are necessary for conversion at lower densities, but the number of days remains unchanged. Vessel dormancy (time that the vessel can absorb heat from the environment before having to vent fuel to avoid exceeding vessel rating) increased between 3 and 7 days depending on hydrogen density, therefore indicating a potentially large benefit for reduced fuel venting in cryogenic pressurized hydrogen storage.

1. Introduction

Storing hydrogen on-board a vehicle presents many challenges, such as safety, cost and compactness. Although the low temperature and high density of liquid hydrogen (LH₂) offer interesting features for safe and long range hydrogen vehicles, boil-off losses have been a limiting factor for the application [1]. In order to address this issue, cryogenic pressure vessels have been developed over the last decade ([2], [3], [4],[5]). Cryogenic pressure vessels are rated for high pressure (350 bar vs. 6 bar in LH₂ automotive vessels [6]) and can therefore contain the hydrogen even as it heats up and pressurizes due to heat transfer from the environment. When H₂ is extracted during driving, the remaining H₂ in the vessel expands isentropically, cooling down in the process. Isentropic cooling becomes more effective as vessel temperature increases. Therefore, vessels that warm up due to infrequent use will cool down the most. Very little driving (a few miles per day) will therefore suffice to stay within the vessel’s rated pressure. As a

consequence, the dormancy (time for which a cryogenic vessel can absorb heat from the surroundings without venting to avoid exceeding the rated pressure) increases considerably, and venting losses are eliminated for typical vehicle utilization scenarios.

Because cryogenic pressure vessels operate over a wide range of pressures and, more importantly, temperature (from 20.3 K to 300 K, and above), they are more likely to take advantage of one of the unique thermal properties of hydrogen: the conversion of the quantum spin states of the molecule. The H₂ molecule is homonuclear and therefore its rotational wave function can be symmetric or antisymmetric, the two quantum states being respectively described as ortho and para. The antisymmetric (para) form has lower internal energy than the symmetric (ortho) form, and their distribution is a function of temperature: almost all molecules are para-H₂ at equilibrium at liquid temperature (20.3 K), while the ortho-H₂ fraction becomes 75% at room temperature. As H₂ warms up in the cryogenic pressure vessel, para-ortho H₂ conversion would therefore take place and absorb energy, thus reducing the pressure and temperature rise (hence the boil-off losses), improving the overall dormancy performance.

In this paper, we examine the kinetics of natural para-ortho H₂ conversion in a full-scale automotive cryogenic pressure vessel rated for 345 bar. After a brief theoretical background on para and ortho-H₂ fundamentals and the effect of the conversion on the thermodynamics of cryogenic pressure vessels, we present measurements of para-ortho H₂ fraction vs. time for densities between 14 and 67 g/L, up to 345 bar and 300 K. The kinetics of the conversion is then analyzed and the resulting heat absorption described.

2. Theoretical background

In quantum mechanics, the (complex) wave function ψ represents a solution to Schrodinger's equation and describes the behavior of a system. In particular, the probability density function (i.e. the probability of finding the particle at any given location and time) can be calculated as the product of the wave function and its complex conjugate $\psi\psi^*$.

The wave function for a hydrogen molecule is the product of five functions [7]:

$$\psi = (\textit{electronic orbital motion})(\textit{electronic spin}) \\ (\textit{nuclear vibrational})(\textit{nuclear rotational})(\textit{nuclear spin}) \quad (1)$$

In accordance with Pauli's exclusion principle, it has been observed that the wave function for the hydrogen molecule (Equation 1) is antisymmetric in the proton coordinates (i.e. the wave function changes sign when the two protons are exchanged). Separately considering each of the five factors in Equation (1), it can be shown that the first three factors are symmetric with respect to a proton exchange. Considering that the total wave function is antisymmetric, the last two factors in Equation (1) necessarily have opposite symmetries. Two possibilities exist [8]:

1. Para-hydrogen: symmetric nuclear rotation and antisymmetric nuclear spin
2. Ortho-hydrogen: antisymmetric nuclear rotation and symmetric nuclear spin

The rotational wave function for the hydrogen molecule using the rigid rotator approximation is symmetric for even J and antisymmetric for odd J , where J is the eigenvalue (quantum number) for the rotational wave function solution. Therefore, para (ortho)-H₂ has an even (odd) rotational quantum number J . The partition function for each rotational state is written as [9]:

$$Z(\text{even, rot}) = \sum_{J \text{ even only}} (2J + 1) \exp\left(-\frac{BJ(J + 1)}{k_B T}\right) \quad (2)$$

$$Z(\text{odd, rot}) = 3 \cdot \sum_{J \text{ odd only}} (2J + 1) \exp\left(-\frac{BJ(J + 1)}{k_B T}\right) \quad (3)$$

Where B is the rotational constant and k_B the Boltzman constant. The “3” in equation (3) is the result of the 3-fold degeneracy associated with the (triplet) odd- J states (from quantum mechanics, there are three degenerate spin (triplet) states for every antisymmetric (singlet) spin state for a pair of interacting spin $\frac{1}{2}$ particles). Equations (2) and (3) can directly be derived into the equilibrium molar fraction of even- J (or “para”) and odd- J (or “ortho”) states population (see equation (4) for the equilibrium fraction of ortho-H₂) and thermodynamic properties such as the rotational energy (see equation (5)) [9]:

$$c_e = 100 \frac{Z(\text{odd, rot})}{Z(\text{odd, rot}) + Z(\text{even, rot})} \quad (4)$$

$$E_{rot} = k_B T^2 \frac{\partial \ln Z}{\partial T} \quad (5)$$

At elevated temperature ($T > 300$ K) where all the rotational energy levels are populated, H₂ equilibrium composition is 75% ortho-H₂ and 25% para-H₂. This mixture is typically named “normal H₂.” At low temperature, thermodynamic equilibrium shifts toward the lower energy form ($J=0$, para-H₂), and the equilibrium fraction at LH₂ saturation temperature at 1 bar (20.3 K) is almost pure para-H₂ (99.7% [8]). Figure 1 shows para-ortho H₂ equilibrium, and rotational energies of ortho-H₂ and para-H₂, as a function of temperature calculated from Eq. (4) and (5). The para-ortho H₂ conversion ($E_{\text{conversion}}$) is the difference between the rotational energies.

Conversion between ortho and para-H₂ is, however, very slow because such a transition results only from perturbations involving nuclear spins, and these are small in magnitude. Therefore, if not catalytically assisted, ortho-H₂ remains unconverted during liquefaction even as LH₂ temperature is approached. If normal H₂ is liquefied, ortho-H₂ will then slowly convert to para-H₂ over many days, liberating enough heat to vaporize 65% of the LH₂ [10], even if the LH₂ remains perfectly insulated.

Catalytic ortho-para H₂ conversion is therefore necessary for efficient liquefaction. Metastable ortho-H₂ is brought into equilibrium through interaction with strong magnetic field gradients. For example, paramagnetic impurities [11], electric discharges [12], atoms formed by thermal dissociation [13], metal catalysts [14] or radiation [15] are all known to increase the ortho-para H₂ conversion rate. Ortho-H₂ itself is also a (slow) catalyst. Ortho-H₂ has a nuclear spin magnetic

moment, and causes $J=1$ de-excitation of neighboring molecules through bimolecular collisions due to interaction between the nuclear magnetic moment and the magnetic moment of the rotating molecule [16]:

p (6)

When normal H_2 is cooled from room temperature and liquefied and an appropriate catalyst is used, between 100 and 708 kJ/kg is released during ortho-para H_2 conversion [17], depending on the temperature (Figure 1). By comparison, the enthalpy of vaporization of LH_2 at atmospheric pressure and 20.3 K is 445.4 kJ/kg [18]. In a liquefaction plant, conversion energy needs to be removed to cool down the mixture and avoid vaporization, thereby increasing energy consumption [19].

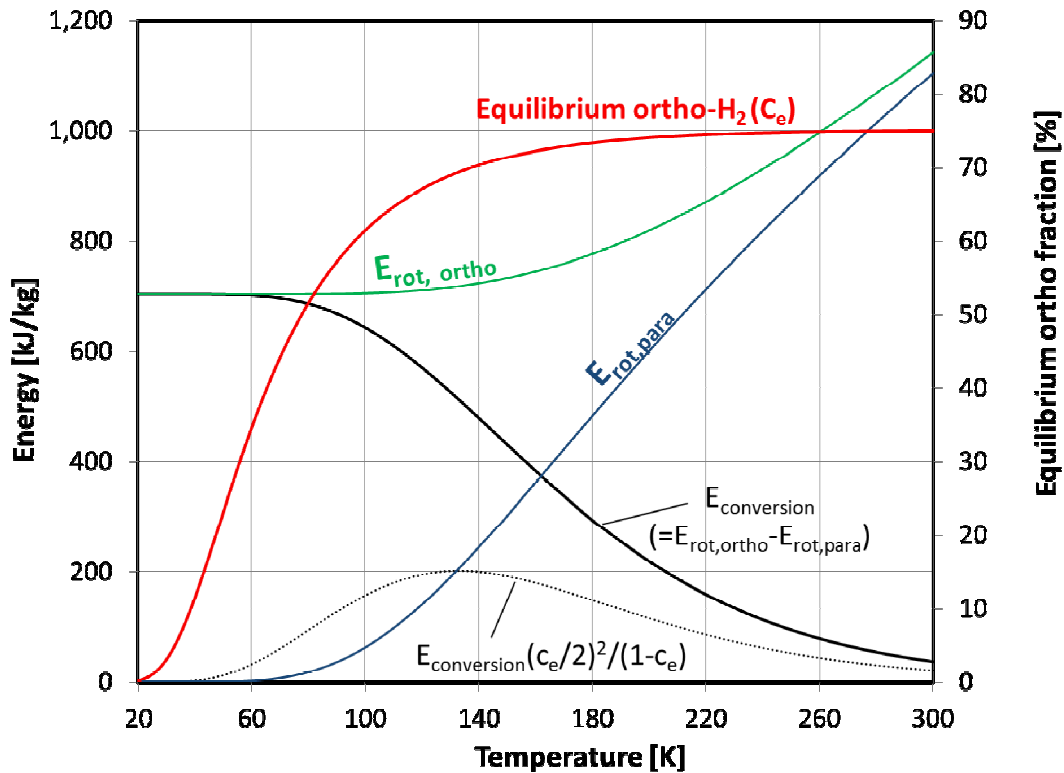


Figure 1. Equilibrium ortho- H_2 fraction (red), energy of para-ortho H_2 conversion (black), rotational energy of ortho- H_2 (green) and para- H_2 (blue), and maximum cooling from para-ortho H_2 conversion, given as $E_{\text{conversion}}(c_e/2)^2/(1-c_e)$ (see text for details), all as a function of temperature.

Ortho-para H_2 conversion kinetics has been carefully studied because it is critical to efficient liquefaction. However, conversion kinetics of the reverse *para-ortho* H_2 reaction has until recently lacked practical interest because hydrogen has always been stored at near constant temperature (as a liquid at 20.3 K and 99.8% para- H_2 , or as compressed gas at room temperature and 75% ortho- H_2 and 25% para- H_2) where para-ortho H_2 conversion is unlikely to occur.

Cryogenic pressurized H₂ storage, on the other hand, operates at varying temperatures, cooling down when frequently driven and warming up when parked. Equilibrium para-ortho H₂ fraction may therefore vary substantially depending on the details of vehicle utilization. In particular, when the vessel heats up due to infrequent driving, equilibrium shifts from para to ortho-H₂ - an endothermic reaction that may absorb a non-negligible amount of energy, reducing the pressurization rate and the potential for fuel venting. Para-ortho H₂ conversion is therefore synergistic with the storage needs of cryogenic pressurized H₂ storage.

In the absence of an external catalyst, the kinetics of natural (*self-catalyzed*) para-ortho H₂ conversion (Equation 7) can be expressed as [20]:

$$\frac{\partial c}{\partial t} = -kc^2 + k'c(1 - c) \quad (7)$$

where c is the ortho-H₂ fraction, k is the kinetic constant of the forward reaction (ortho-para), and k' is the kinetic constant of the backward reaction (para-ortho).

At equilibrium, the variation of ortho-H₂ is null. Therefore, k and k' are related by:

$$k' = \frac{kc_e}{1 - c_e} \quad (8)$$

where c_e is the equilibrium fraction of ortho-H₂ (a function of temperature, Figure 1).

Equation (7) can then be written as:

$$\frac{\partial c}{\partial t} = -\frac{kc(c - c_e)}{1 - c_e} \quad (9)$$

For a given k , the rate of change of the ortho-H₂ fraction is maximum for $c=c_e/2$ (condition for which the second derivative of c vs. time is equal to zero). For $c=0$ (no ortho molecules in the system) and for $c=c_e$ (equilibrium), the rate becomes zero: conversion cannot take place.

While several fundamental studies have been performed on para-ortho H₂ conversion in the solid phase, surprisingly few studies exist on conversion kinetics of fluid H₂ in the supercritical region. The earliest known studies of para-ortho H₂ conversion kinetics in isothermal liquid H₂ were from Cremer and Polanyi [20], who found a rate constant $k=12 \times 10^{-3} \text{ hr}^{-1}$ at 20 K. Around the same time it was suggested by Wigner [21] that the rate constant would be sensitive to density and temperature ($k \sim \rho T^{-1/2}$) in the presence of paramagnetic impurities. More recently, Milenko et al. [22] presented ortho-para H₂ conversion data on both liquid (17-32 K) and supercritical (40-120 K) H₂ up to 92 g/L density based on H₂ thermal conductivity measurements. A semi-empirical model was then derived which supplemented Wigner's model by considering the

velocity dependence of the approach distance between colliding molecules. Milenko's correlation for the kinetic rate is given in units of 10^{-3} h^{-1} as a function of temperature and density as:

$$k = (18.2 \pm 1.6)T^{0.56 \pm 0.02}\rho + 5.10^4(0.77 \pm 0.03 + (921 \pm 94)T^{-2.5 \pm 0.2})\rho^{3.6} \quad (10)$$

While the conversion rate constant was observed to scale (roughly) linearly with density, their data showed an increase in conversion rate with temperature, in contrast to the $\sim \rho T^{-1/2}$ law expected from Wigner's theory.

Finally, Matthews et al. [23] studied natural para-ortho H_2 conversion for temperatures between 32 and 280 K and densities between 14 and 60 g/L, and showed similar temperature variability as Wigner's original paramagnetic theory. Some of the results from this work are used here to study their effect on the thermodynamic behavior of cryogenic pressurized H_2 storage.

3. Cryogenic Pressure Vessel Thermodynamics

For a closed H_2 vessel of constant volume, mass (noted m), and baseline environmental heat transfer rate Q , the conservation of internal energy E is written as:

$$m \frac{dE}{dt} = Q \quad (11)$$

Thus:

$$m \left[(1 - c) \frac{dE_{\text{para}}}{dt} + c \frac{dE_{\text{ortho}}}{dt} \right] = Q - m(E_{\text{ortho}} - E_{\text{para}}) \frac{dc}{dt} \quad (12)$$

Using Eq. (9), the variation of the internal energy of a constant density H_2 mixture including natural para-ortho H_2 conversion becomes:

$$m \left[(1 - c) \frac{dE_{\text{para}}}{dt} + c \frac{dE_{\text{ortho}}}{dt} \right] = Q + mE_{\text{conversion}} \frac{kc(c - c_e)}{1 - c_e} \quad (13)$$

As previously stated, para-ortho H_2 conversion is fastest for $c=c_e/2$. The maximum cooling due to para-ortho H_2 conversion is thus $E_{\text{conversion}}(c_e/2)^2/(1-c_e)$. This is shown in Figure 1 as a function of temperature.

E_{para} and E_{ortho} are derived from temperature and pressure using the 32 term modified Benedict-Webb-Rubin equation of state as implemented in REFPROP [24]. This database has been shown [25] to adequately determine isomer transitions properties in H_2 assuming they are adjusted to a common reference state.

Equation (13) predicts the rate of change in internal energy, and thus directly governs vessel temperature (and pressure) rise. The right-hand side of Equation (13) is named *apparent heat*

transfer and it gives an indication of the impact of para-ortho H₂ conversion vs. heat transfer from the environment.

Consider now the theoretical effect of para-ortho H₂ conversion on LLNL's experimental cryogenic pressure vessel with 151 liters, 345 bar rating, 5 Watts heat transfer, initially filled with 50 g/L of saturated LH₂ at atmospheric pressure and 20.3 K [4]. Figure 2 shows pressure, temperature, apparent heat transfer, and ortho-H₂ fraction as a function of time for three different cases: (a) no para-ortho H₂ conversion, (b) para-ortho H₂ conversion at the kinetic rate defined by Milenko et al. [22], and (c) infinitely fast conversion, $c=c_e$. Results show that Milenko's kinetics predicts a time lag of 10 to 12 days before conversion starts, and that conversion is almost complete in 25 days. The conversion temperature is ~115 K. Vessel rated pressure (345 bar) is reached in about 12 days if no para-ortho H₂ conversion takes place (case a). Thus H₂ venting would then take place. Para-ortho H₂ conversion lengthens dormancy by 8 days according to Milenko's kinetics, case (b). The infinitely fast rate for case (c) lengthens dormancy even more. Apparent heat transfer (baseline environmental heat transfer minus heat absorbed by para-ortho H₂ conversion) is predicted to be negative during day 18, cooling and depressurizing the vessel even as heat transfer from the environment continues.

Based on these preliminary calculations, it appears that para-ortho H₂ conversion may play a significant role in lengthening the dormancy of full-scale cryogenic pressure vessels. Experimental results are necessary to validate these modeling results.

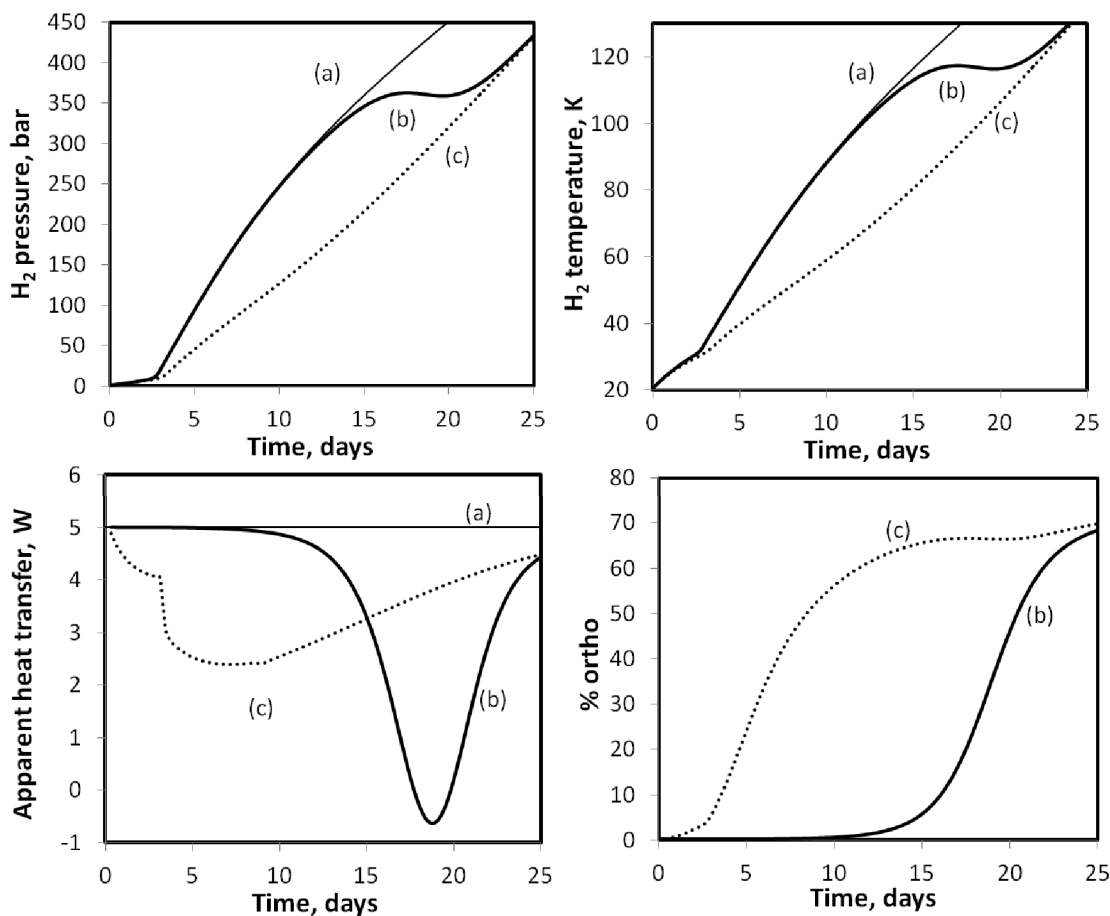


Figure 2. H₂ pressure, temperature, apparent heat transfer, and ortho-H₂ fraction as a function of time, for a cryogenic vessel with 50 g/L and 5 Watts heat transfer for three cases: (a) no conversion (pure para-H₂) (b) Milenko's kinetics [22], and (c) thermodynamic equilibrium (infinitely rapid kinetics).

4. Experiments

Experiments were conducted in LLNL's 345 bar cryogenic vessel with 151 L internal volume installed onboard a modified hydrogen-fueled Toyota Prius (Figures 3 and 4). A silicon diode (TC3 in Figure 3) measured temperature to an accuracy better than 0.12% while the pressure transducer (PT2 in Figure 3) has +/-1.7 bar accuracy. H₂ density was derived from measured pressure and temperature using the Younglove equation of state [26]. Uncertainties in density for the equation of state are 0.1% in the liquid phase, 0.25% in the vapor phase, and 0.2% in the supercritical region.

Two methods were used for determining ortho-H₂ fraction: rotational Raman spectroscopy and calorimetry. For rotational Raman spectroscopy we collected H₂ samples from the experimental vessel through the relief line (Figure 3). The initial step was venting a small amount of H₂ ($\Delta p < 0.6$ bar) to flush the vent tube and guarantee that analyzed samples were representative of the bulk H₂ contained in the vessel. Samples were then collected through a bleed valve into a 12.5 mm diameter 60 mm long copper Raman cell equipped with 5 mm thick fused silica windows

(Figure 4, right). Figure 5 shows the main steps required for data collection and analysis. Because the sampled gas quickly comes to thermal equilibrium, the non-equilibrium ortho-para mixture immediately begins to slowly convert. Therefore, rapid transfer of the sample from the vessel test area to the Raman spectroscopy lab was essential. The exact transfer times were logged in order to assess possible errors in kinetic coefficient estimation.

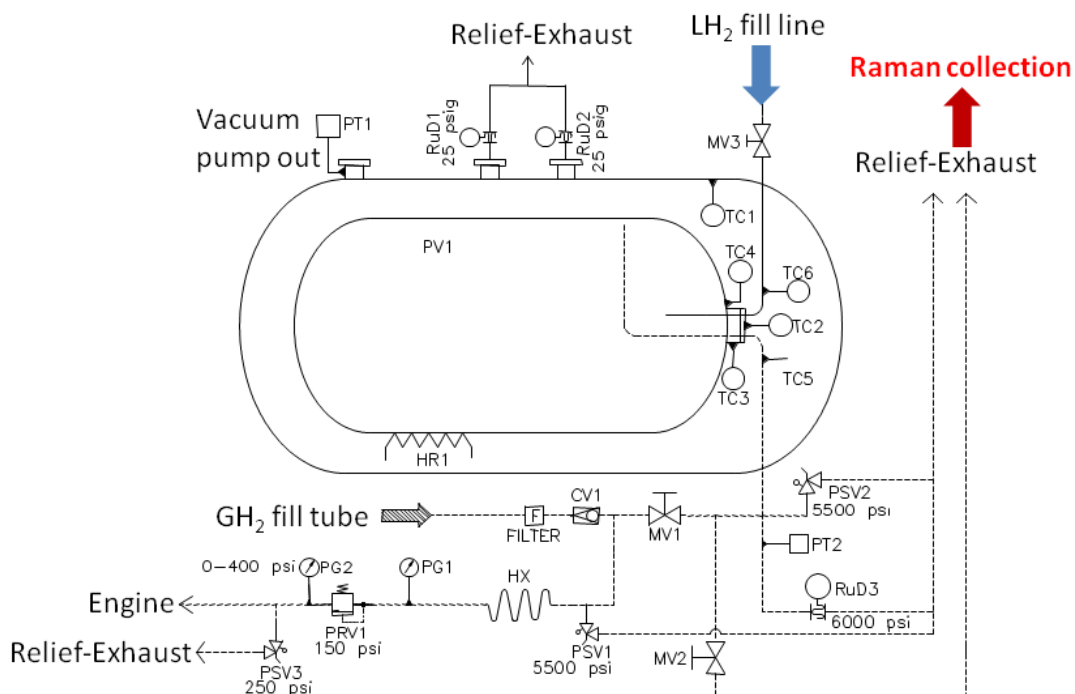


Figure 3. Piping and instrumentation diagram of the 151 L, 345 bar Cryogenic Pressure Vessel. Hydrogen samples are collected through the relief line by opening valve MV2.



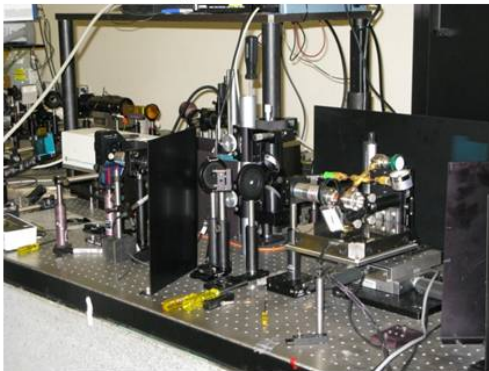
Figure 4. Sample collection for rotational Raman spectroscopy on the experimental hydrogen-fueled Toyota Prius equipped with a 151 L, 345 bar cryogenic pressure vessel.



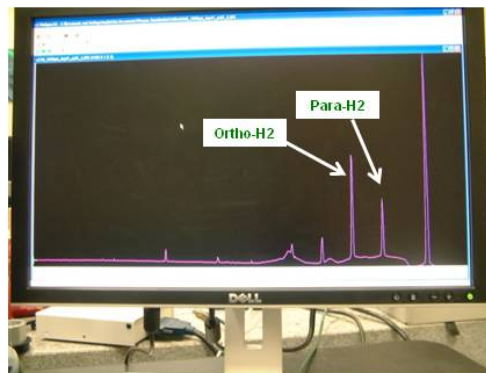
Sample collection



Rapid delivery (~10 min) to laser lab



Laser Raman analysis



Spectrum results

Figure 5. Experimental protocol for measuring para-ortho H₂ fraction using rotational Raman spectroscopy

Raman scattering measurements were carried out using a diode-pumped frequency-doubled Nd:YVO₄ CW (continuous wave) laser operating at 532 nm in a back-scattering confocal collection geometry. Laser light enters through a window in the Raman cell and the light is analyzed after interacting with the hydrogen (Figure 6). Most of the light leaving the Raman cell has the same frequency as the laser (Rayleigh scattering). 532±5 nm light is blocked using an optical notch filter allowing only inelastically scattered light of different frequencies into our collection optics. A very small portion of the incident laser photons give up some of their energy to the various rotational-vibrational manifolds of the hydrogen molecules. Thus they scatter with slightly less energy and are therefore shifted to slightly longer wavelengths. This is the Raman Effect. The amount of spontaneous Raman scattered light is directly proportional to the number of molecules in each rotational energy state. Each energy state yields a slightly different Raman wavelength. Thus we can make a direct measurement of the relative populations of para and ortho H₂ molecules.

Filtered Raman light was dispersed through an f/4 spectrometer onto a liquid nitrogen-cooled 1100x330 pixel back-illuminated Charge Coupled Device, yielding a spectral resolution and accuracy of ~4 cm⁻¹ and <1 cm⁻¹. A quartz-tungsten-halogen lamp was used for absolute intensity calibration. The total integration time for each spectrum was 60 s.

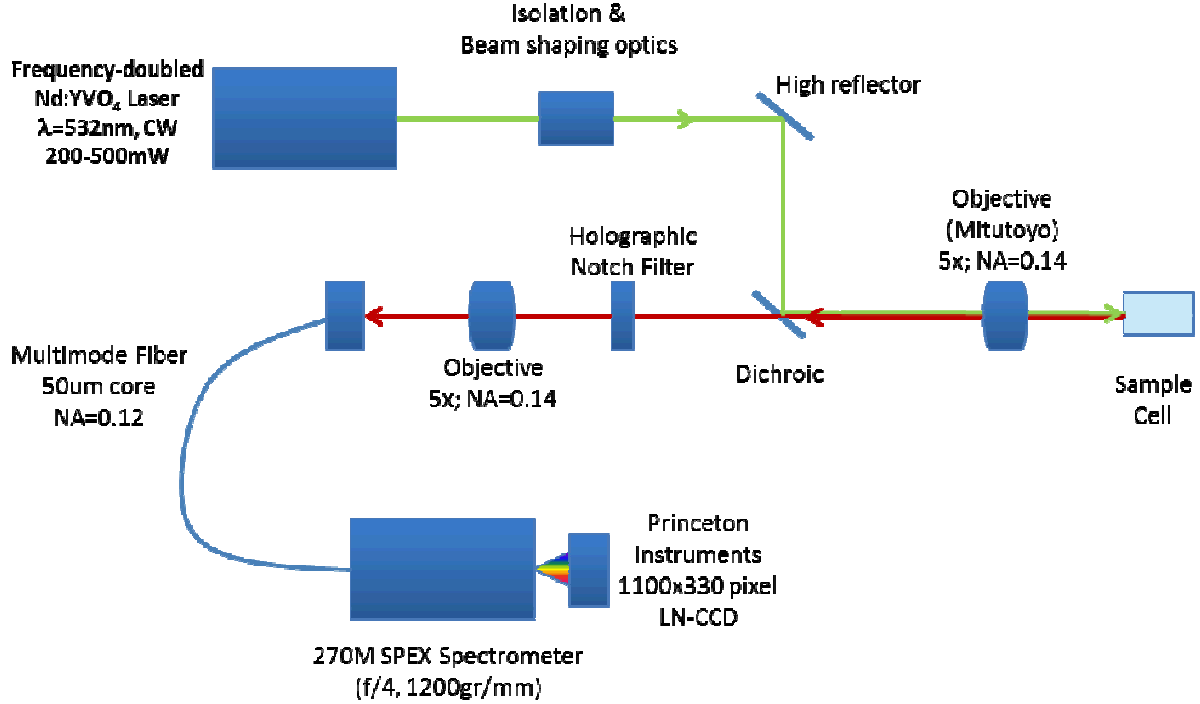


Figure 6. Schematic of the confocal Raman microscopy setup for measuring para/ortho- H_2 fractions.

Figure 7 shows the observed change in H_2 rotational Raman scattering measured from samples taken between 72 and 168 K for a vessel with 51 g/L H_2 . Between 200 and 700 cm^{-1} two peaks at 354 and 587 cm^{-1} are observed corresponding to the $S_0(0)$ rotational transition ($J=2 \leftarrow 0$) of para- H_2 and the $S_0(1)$ transition ($J=3 \leftarrow 1$) of ortho- H_2 respectively. Raman peaks corresponding to $S_0(2)$ and $S_0(3)$ transitions (>700 cm^{-1}) were observed but not used for relative fraction measurements. The observed Raman bands were well fit (least-squares) to a Gaussian, from which the area of each peak was numerically evaluated. The fraction x_J of para- ($J=0$) and ortho- H_2 ($J=1$) isomers was derived from integrated scattering intensities I_J given proportionally by

$$I_J = \frac{(J+1)(J+2)}{(2J+1)(2J+3)} x_J p_J \gamma_J^2 \omega_s^3 \quad (14)$$

where p_J is the Boltzmann-distributed population of the initial J^{th} level (at room temperature, $T=295$ K), γ_J is the anisotropy of the polarizability tensor and ω_s is the scattered light angular frequency. A sample of normal H_2 (ortho-para ratio of 3:1) was used to verify our method, yielding a value of $x_0=0.752 \pm 0.026$.

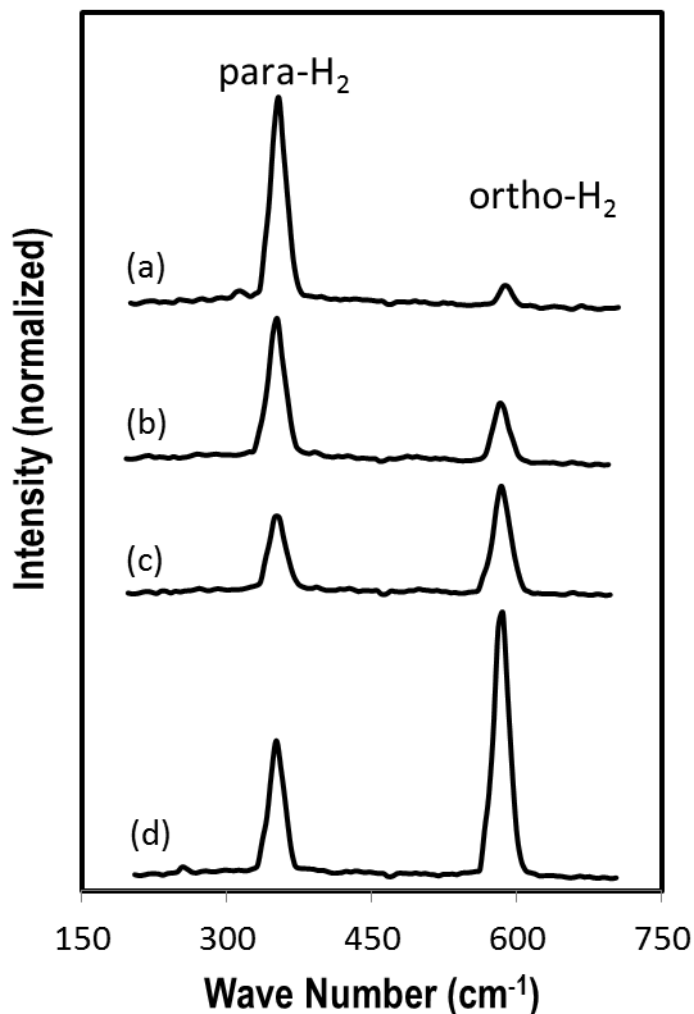


Figure 7. Rotational Raman spectra of H₂ for 51.3 g/L density, at (a) 72 K, (b) 88 K, (c) 114 K, and (d) 168 K. Spectra are normalized for the applied laser power, baseline corrected, and offset vertically for clarity.

Ortho-H₂ fraction was also calculated from calorimetry. The *apparent* heat transfer rate, defined as the right hand side in Equation 13 and representing the heat transfer rate that would reproduce the experimental rate of vessel pressurization in the absence of any para-ortho H₂ conversion, is first determined from pressure and temperature measurements. Considering that environmental heat transfer is fairly constant throughout the experimental runs (except for day and night cycles), para-ortho H₂ conversion can be calculated by subtracting the baseline environmental heat transfer rate minus the apparent heat transfer rate, and dividing this energy deficit by the internal energy of para-ortho H₂ conversion (Figure 1). Although less accurate than Raman spectroscopy due to uncertainty in environmental heat transfer measurements, this method is used as an independent verification of rotational Raman spectroscopy results.

An important concern about this study on natural para-ortho H₂ conversion kinetics is the possible effect of catalysis near the aluminum vessel wall. If near-wall catalysis and molecular

diffusion were rapid enough within the hydrogen vessel (as compared to typical timescales of natural para-ortho H₂ conversion), this “catalytic” reaction would be predominantly observed experimentally instead of the intrinsic effect. To explore this possibility, we modeled the diffusion time of molecular ortho-H₂ across the dimensions of the vessel using the Stokes-Einstein equation and Fick’s law. By fixing the initial slope of the modeled extrinsic conversion to our observed values, we find that this diffusive-catalytic effect is negligible above ~1% ortho-H₂ fractions. Kinetic rate constants obtained at ortho-H₂ fraction lower than 1% should thus be disregarded.

5. Experimental Results

The effect of natural para-ortho H₂ conversion on the thermodynamic behavior of a cryogenic pressure vessel was investigated through a series of experiments spanning 10 months at H₂ densities between 13.8 and 67 g/L, and temperatures between 21.4 and 300 K. Table 1 summarizes the experimental conditions.

Table 1. List of fifteen para-ortho H₂ conversion experiments conducted between March 2010 and February 2011.

Exp.	Date	Density [g/L]	Temperature [K]	Initial ortho fraction [%]	Final ortho fraction [%]	Duration [days]
1	March 2010	67	23.2-68	<0.3	0.3	8.5
2	March/April	60-50	61.5-116	0.3	63	22
3	April	11.8	58.5-97	63	60	2.5
4	May/July	14	20.3-300	<0.3	75	52
5	July/August	51.4	21.4-113	<0.3	58	18
6	August/September	23	76-278	58	75	40
7	September/October	51.4	21.2-109	<0.3	52	20
8	October	13.8	53-195	52	72	14
9	October/November	51.3	21.2-108	<0.3	60	23
10	November	13.8	55-123	60	61.5	7
11	November/December	61.2	21.2-85	<0.3	19.2	17
12	December	51.8	75-106.9	19.2	58	11
13	December	13.8	58.8-170	58	69	14
14	January 2011	62.4	21.1-75.5	<0.3	4	10
15	January/February	28	40-227	4	73	35

Experiments 1, 4, 5, 7, 9, 11, and 14 started with a fresh LH₂ charge at 2-3 bar, 20.3-25 K, and <0.3% ortho-H₂ fraction. The other experiments started after some of the initial H₂ was vented,

typically because the vessel's maximum working pressure (345 bar) was reached. For these experiments, the initial ortho-H₂ fraction equals the final ortho-H₂ fraction of the previous experiment.

Figures 8-14 show H₂ temperature (blue line), equilibrium ortho-H₂ fraction (thin red line) calculated from measured temperature, measured ortho-H₂ fraction from Raman spectroscopy (red circles), and modeled ortho-H₂ fraction (thick red line) based on Milenko's kinetics [22] all as a function of time.

Analysis of experimental results in Figures 8-14 allows us to draw general guidelines about para-ortho H₂ conversion kinetics in a full scale (151 L internal volume) 345 bar H₂ vessel. First, para-ortho H₂ conversion typically becomes active after 10-15 days of parking, when H₂ temperature reaches 70-80 K. Para-ortho H₂ conversion approaches completion (equilibrium) after 25-30 days when the vessel reaches 100-120 K at ~50 g/L density. Warmer temperatures are necessary for full conversion at lower densities (experiments 4 and 15), but the number of days remains unchanged.

Vessel rated pressure sets a limit to the maximum density that can be used in para-ortho H₂ conversion experiments. Considering that para-ortho H₂ conversion typically approaches completion at 100-120 K, density is limited to 48-54 g/L within the 345 bar vessel limit. This is confirmed by experiments 1, 11, and 14 with 60+ g/L where only partial conversion was achieved before venting became necessary.

It is also observed that Milenko's para-ortho H₂ kinetic model consistently underpredicts reaction rates for all experiments. The validity of the model is discussed in more detail in the next section.

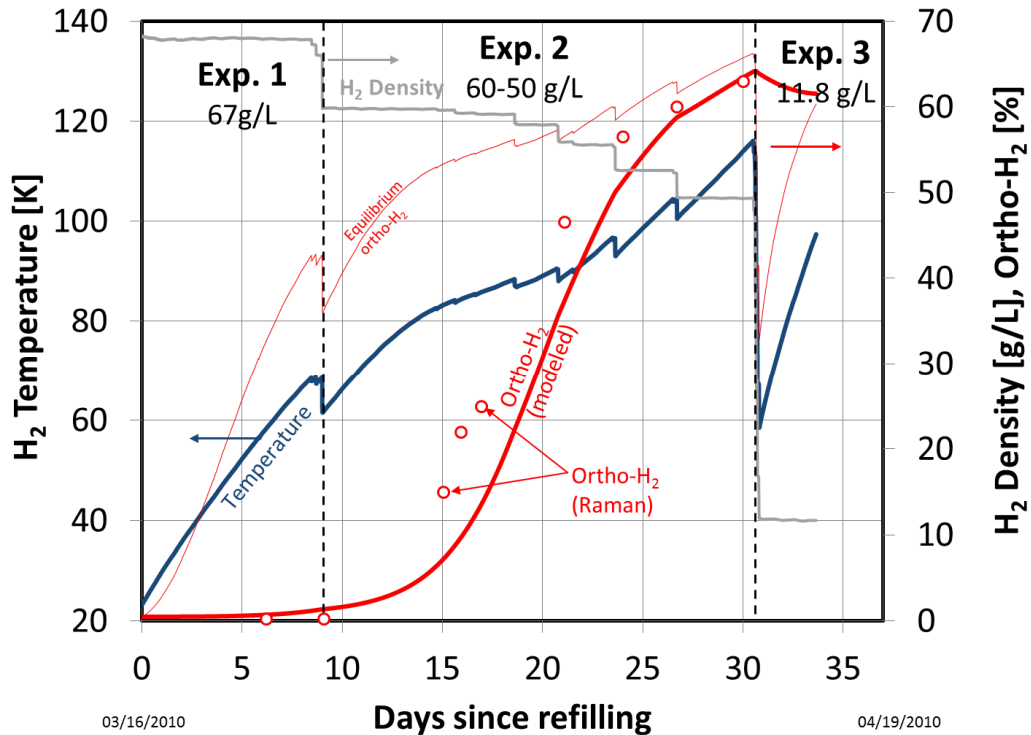


Figure 8. Temperature (blue), density (gray), modeled ortho-H₂ fraction (thick red line), measured ortho-H₂ fraction (red circles), and equilibrium ortho-H₂ fraction (thin red line), as a function of time after the initial fill, for experiments 1-3.

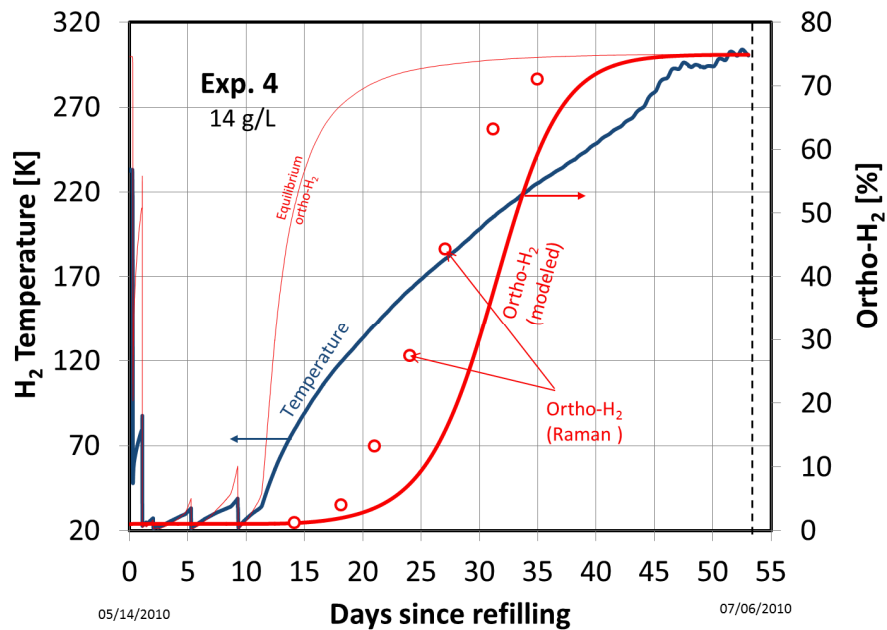


Figure 9. Temperature (blue), modeled ortho-H₂ fraction (thick red line), measured ortho-H₂ fraction (red circles), and equilibrium ortho-H₂ fraction (thin red line), as a function of time after the initial fill, for experiment 4.

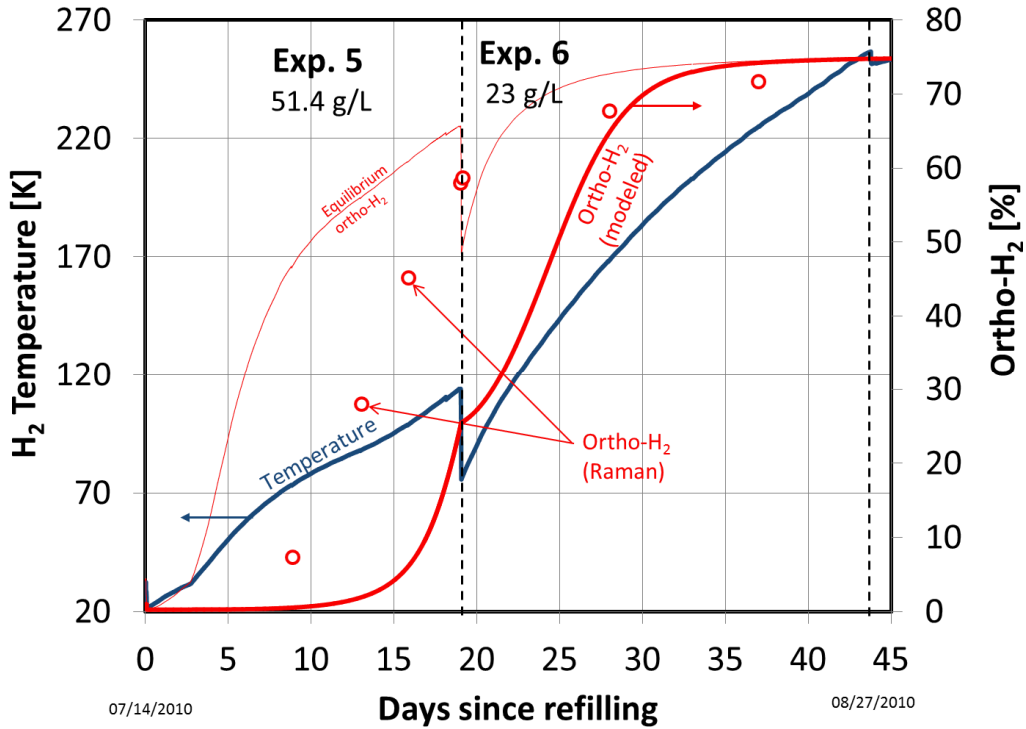


Figure 10. Temperature (blue), modeled ortho-H₂ fraction (thick red line), measured ortho-H₂ fraction (red circles), and equilibrium ortho-H₂ fraction (thin red line), as a function of time after the initial fill, for experiments 5 and 6.

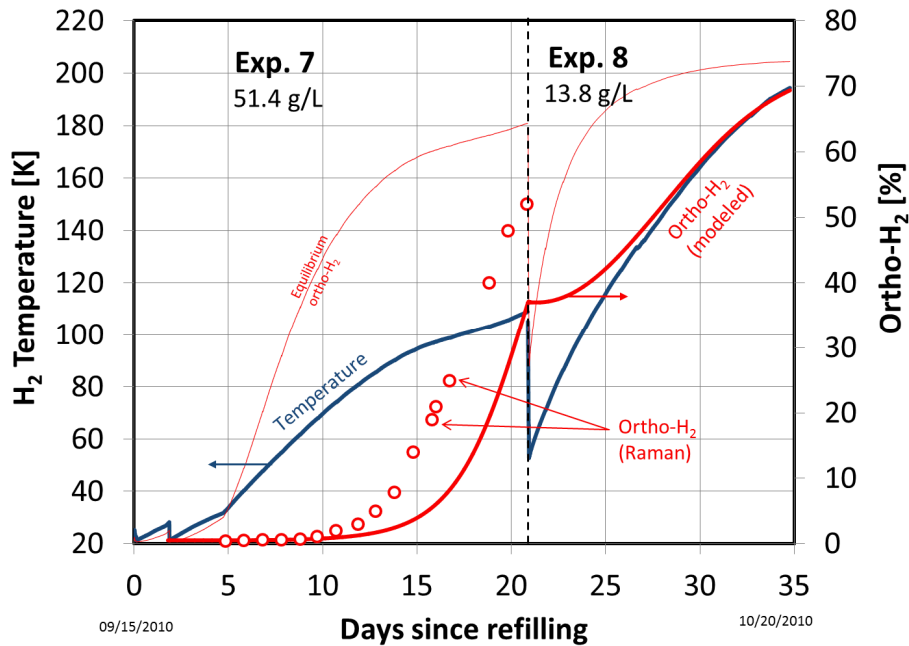


Figure 11. Temperature (blue), modeled ortho-H₂ fraction (thick red line), measured ortho-H₂ fraction (red circles), and equilibrium ortho-H₂ fraction (thin red line), as a function of time after the initial fill, for experiments 7 and 8.

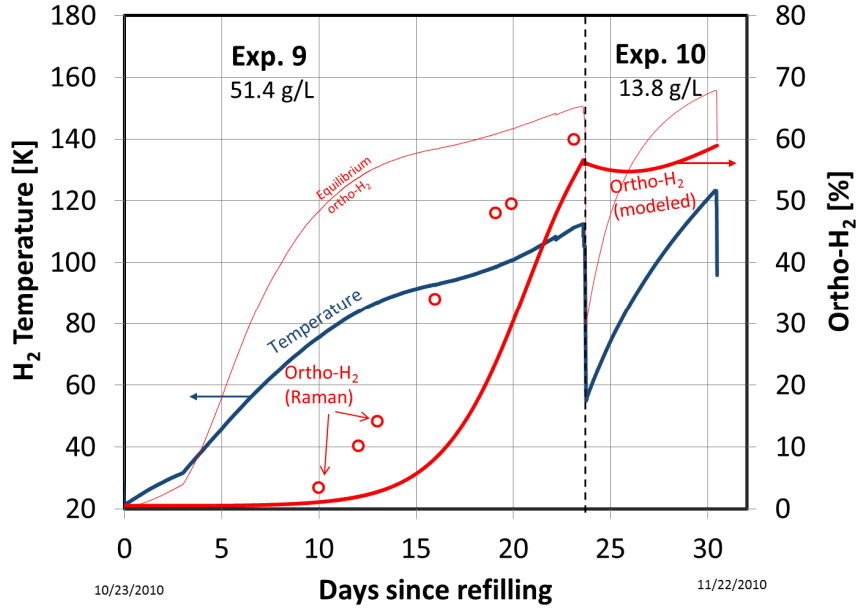


Figure 12. Temperature (blue), modeled ortho-H₂ fraction (thick red line), measured ortho-H₂ fraction (red circles), and equilibrium ortho-H₂ fraction (thin red line), as a function of time after the initial fill, for experiments 9 and 10.

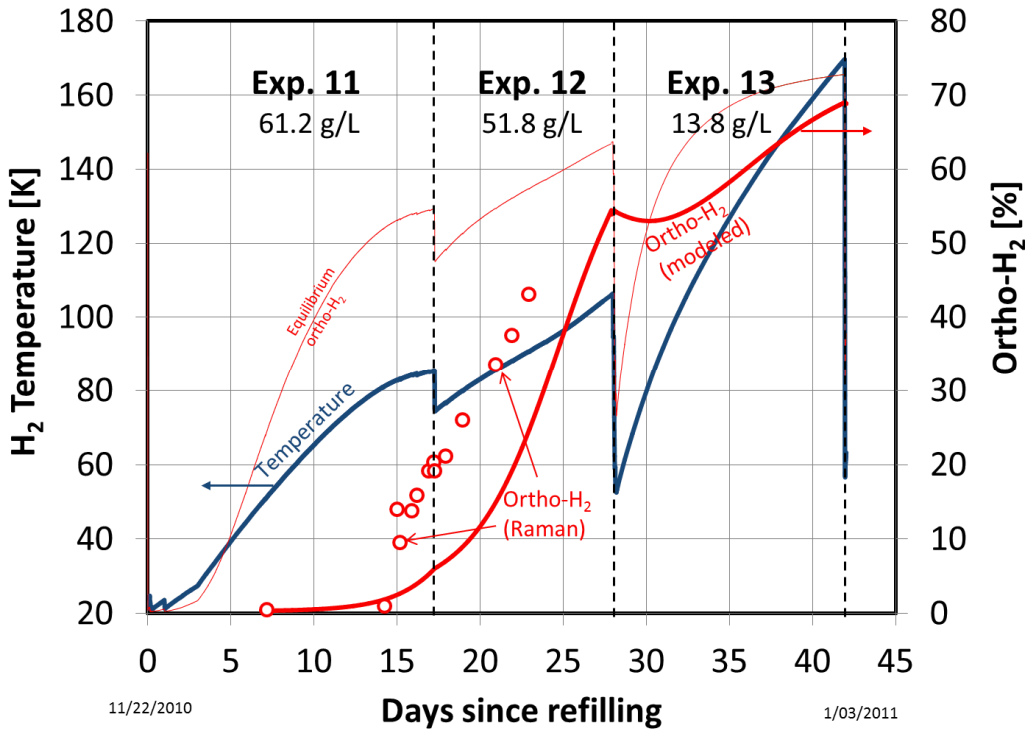


Figure 13. Temperature (blue), modeled ortho-H₂ fraction (thick red line), measured ortho-H₂ fraction (red circles), and equilibrium ortho-H₂ fraction (thin red line), as a function of time after the initial fill, for experiments 11, 12 and 13.

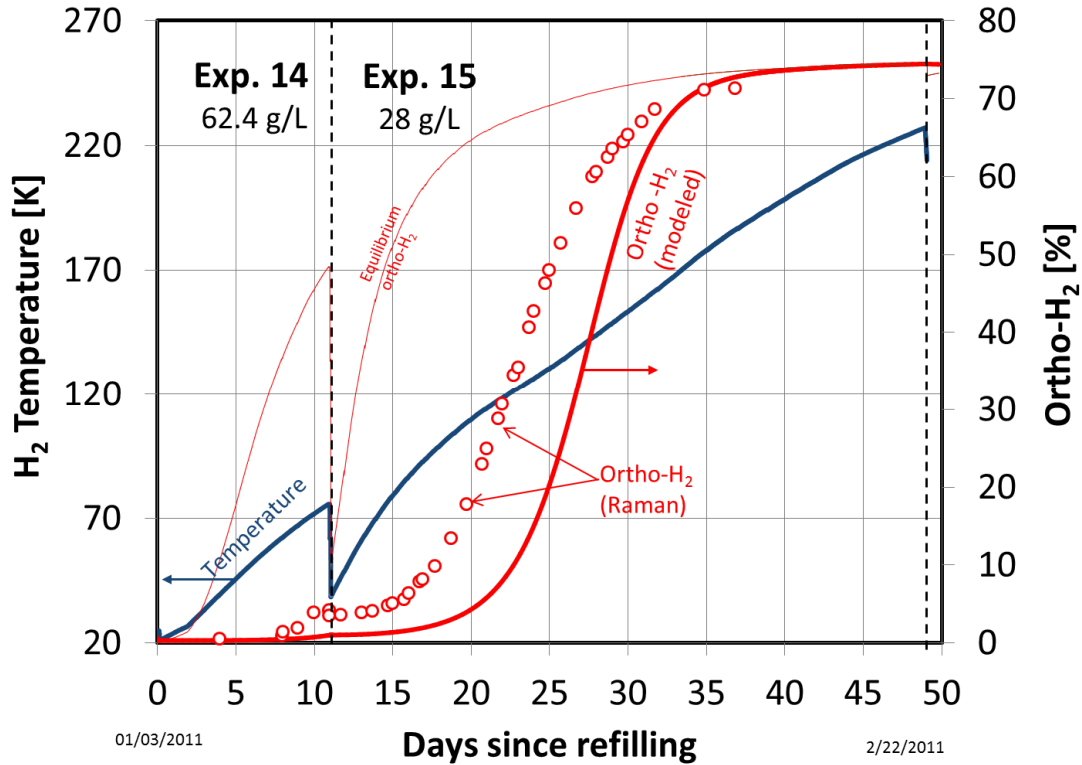


Figure 14. Temperature (blue), modeled ortho-H₂ fraction (thick red line), measured ortho-H₂ fraction (red circles), and equilibrium ortho-H₂ fraction (thin red line), as a function of time after the initial fill, for experiments 14 and 15.

6. Range of validity for Milenko's para-ortho H₂ kinetic correlation

It is important to mention that the semi-empirical expression of the kinetic rate for the conversion between para and ortho-H₂ proposed by Milenko et al. [22] and used for the modeling results in Figures 8 to 14 was elaborated based on the experimental study of the reverse reaction (ortho-para instead of para-ortho) and only for ortho-H₂ fraction between 62 and 75%. In addition to this, Milenko's correlation does not include catalytically enhanced para-ortho H₂ conversion at the vessel walls, which may play a role in building an initial ortho-H₂ concentration. It is therefore not surprising that Milenko's correlation underpredicts para-ortho kinetics at the very low initial ortho-H₂ concentrations presented here.

In this section, we present a qualitative approach to evaluate the range of validity for Milenko's kinetic correlation [22], based on the experimental results of Figures 8 to 14. In this approach, we select experiments with large para-ortho H₂ conversion (experiments 4, 5, 7, 9, 11, and 14), and, for each experiment, we make several runs with a thermodynamic model that includes Milenko's kinetics, starting each of the model runs at experimentally measured pressure, temperature, and ortho-H₂ fraction. We then compare the numerical and experimental results to determine agreement using a coefficient of determination (R^2). For example, consider experiment 4 (Figure 15). In this experiment we made 9 Raman spectroscopy ortho-H₂ measurements in addition to continuous measurements of pressure and temperature. We therefore run the thermodynamic

vessel model 9 times, with initial conditions equal to the measured temperature, pressure and ortho-H₂ fraction.

The results show that Milenko's correlation accuracy increases as ortho-H₂ fraction and temperature increase. For the low density experiment (experiment 4, 14 g/L, Figure 15), 27.5% ortho-H₂ and 163 K are necessary to obtain accurate conversion predictions (within $R^2 > 0.99$). Higher density experiments (e.g. experiment 7, 51.4 g/L, Figure 16), demonstrate accurate prediction at lower temperature and ortho-H₂ (94 K and 14% ortho-H₂). Similar observations have been made for other experiments and the analysis suggests that these threshold values (above which the experimental results agree with the theoretical equations from Milenko) decrease with increasing density (Table 2).

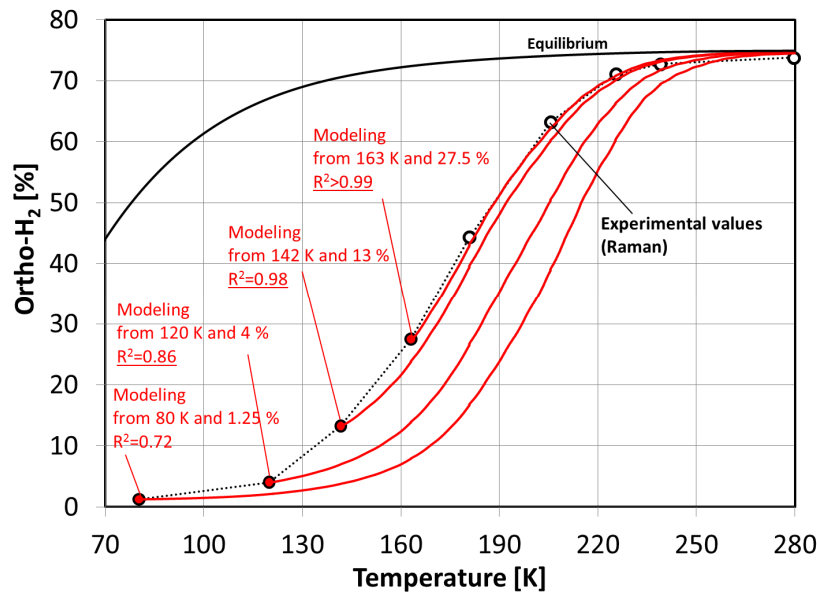


Figure 15. Ortho-H₂ fraction as a function of temperature for experiment 4 (14 g/L). The circles represent experimental values; and the lines are the ortho-H₂ fraction variation calculated using Milenko's correlation [22] from four different starting points. Coefficients of determination (R^2) for each of the modeling runs are also reported.

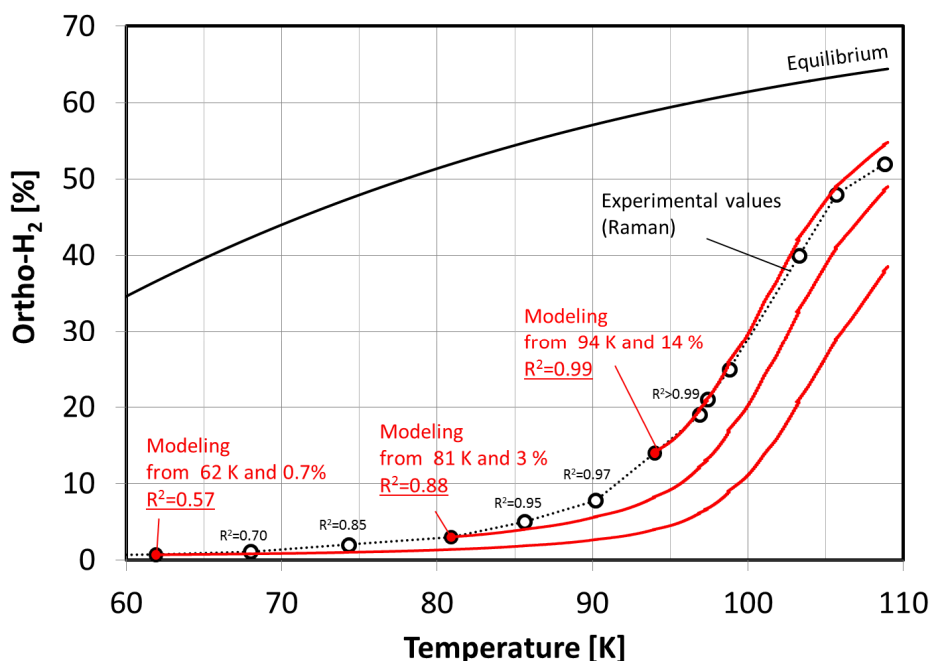


Figure 16. Ortho-H₂ fraction as a function of temperature for experiment 7 (51.4 g/L). The circles represent experimental values; and the lines are the ortho-H₂ fraction variation calculated using Milenko's correlation [22] from three different starting points. Coefficients of determination (R^2) for each of the modeling runs are also reported.

Table 2. Threshold values of temperature and ortho-H₂ fraction above which good agreement ($R^2 > 0.99$), has been found between the experimentally observed kinetic rates and the semi-empirical values from Milenko et al. [22] at 4 different H₂ densities.

H ₂ density	Minimum temperature and ortho-H ₂ fraction [%] above which experimental results agree well with Milenko et al. [22] ($R^2 > 0.99$)
14 g/L	163 K & 27.5 %
28 g/L	108 K & 17 %
51.3 g/L	90 K & 13%
61.2 g/L	75 K & 4 %

It can be shown [23] that while the magnitude of our measured kinetic constants agree well with Milenko's measurements [22], the slight decrease with increasing temperature (Fig. 17) is consistent with Wigner's original theory [21] if we assume unrealistically small collision distances ($\ll 300$ pm) that are required to achieve reasonable values. This might suggest that the collision approach distance dependence on temperature may in fact be somewhat weak, a possibility that may be borne out of more precise calculations of paramagnetic molecular collisions in a dense fluid. An experimental apparatus with independent control of temperature would be necessary in order to further investigate this effect, by decoupling the effects of temperature vs. ortho-H₂ fraction on the kinetic rates. This was, however, not possible in this study.

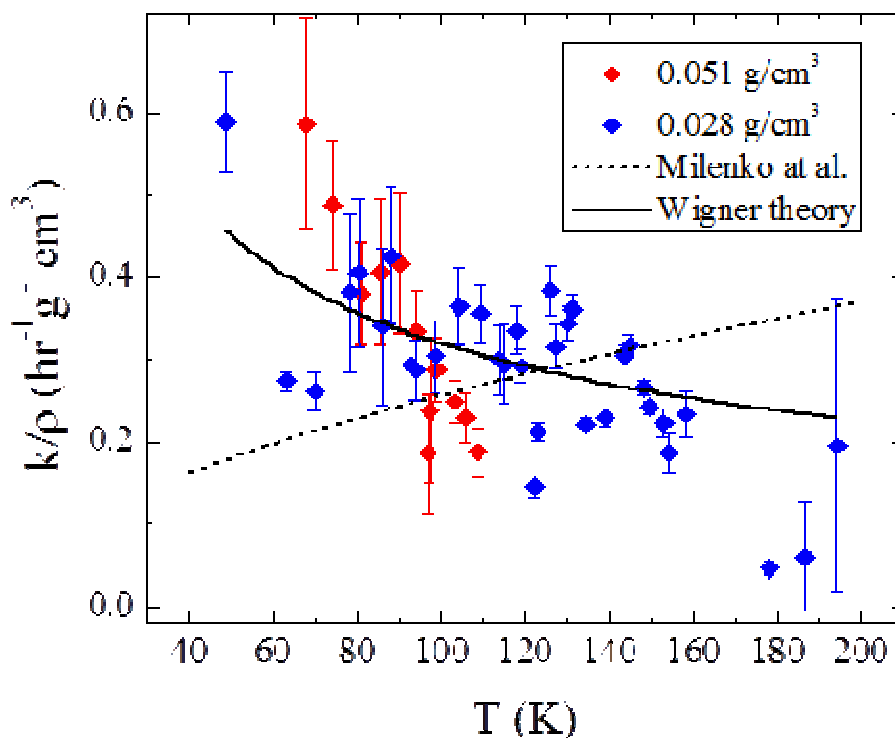


Figure 17. Normalized conversion rate constant k/p vs. temperature for $\rho = 51$ g/L (blue symbol) and $\rho = 28$ g/L (red symbol) compared with Wigner (solid) and Milenko (dashed) model predictions. Please note that the results calculated for Wigner's model assume unrealistically small collision distance ($\ll 300$ pm) in order to obtain reasonable fit to the experimental data. Figure reprinted from [23].

7. Thermodynamic analysis

Knowing the range of validity of Milenko's correlation, it is now possible to conduct thermodynamic analysis with improved predictive accuracy by initializing para-ortho H_2 calculations at the appropriate conditions (Table 2). The results of the analysis can be found in Figures 18-23. These figures show pressure, temperature, ortho- H_2 fraction (measured by Raman spectroscopy and calorimetry, and modeled with Milenko's kinetics, within the range of validity from Table 2) and heat transfer (baseline and apparent) as a function of time for the experiments with the most active para-ortho H_2 conversion rates: experiments 1-3, (Figure 18), experiment 5 (Figure 19), experiment 7 (Figure 20), experiment 9 (Figure 21), experiments 11-13 (Figure 22), and experiment 15 (Figure 23).

The top chart in Figures 18-23 shows baseline (black) and apparent (red) heat transfer into the cryogenic vessel. The figures show daily heat transfer cycles because the experiment was

conducted in the open to analyze real world para-ortho H_2 conversion effect on dormancy. Baseline heat transfer during para-ortho H_2 conversion (“Q” in Equations 11-13) is calculated based on H_2 temperature, environment temperature, and insulation vacuum quality (pressure in the vacuum jacket [10]). The average baseline heat transfer is ~5 Watts. However, greater (up to 7 Watts, Fig. 16) and lower (down to 2.5 Watts, Fig. 20) are noticed. Higher than average heat transfer is due to loss of vacuum quality caused by composite vessel outgassing [5]. Lower than average baseline heat transfer is explained by high hydrogen temperature (up to 220 K, Fig. 23). The green area represents the total energy absorbed by para-ortho H_2 conversion during the experiments. Para-ortho H_2 cooling reduced apparent heat transfer to as little as 1.5 Watts (Figures 18-20). Ortho- H_2 fraction can be calculated from calorimetry (Section 4), by measuring the green area and dividing it by the para-ortho H_2 conversion energy (Figure 1).

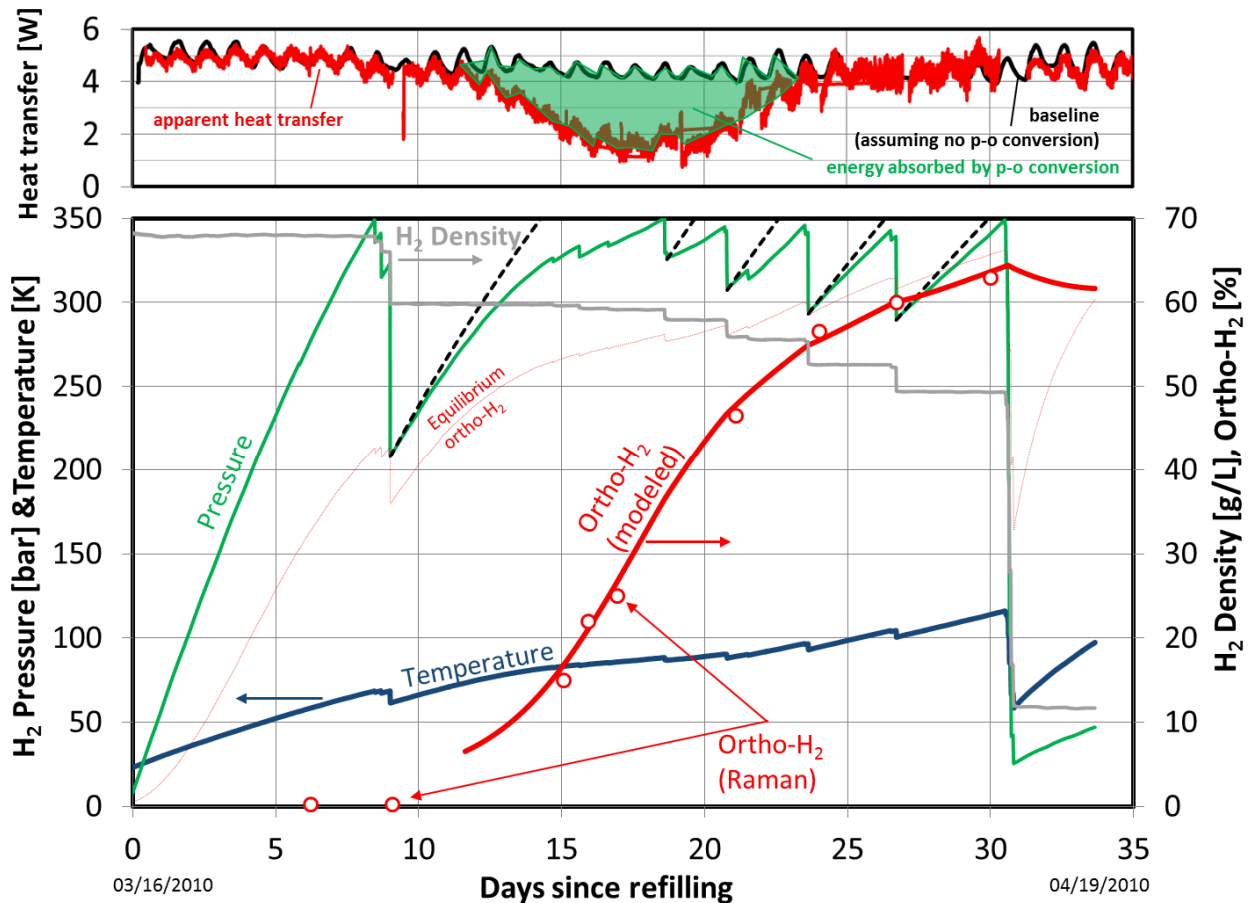


Figure 18. H_2 pressure (green line), pressurization rate with no para-ortho H_2 conversion (black dashed line), temperature (blue line), equilibrium ortho- H_2 fraction (red thin line), measured ortho- H_2 fraction (Raman spectroscopy, red circles), modeled ortho- H_2 fraction (thick red line), H_2 density (thin gray line), and baseline heat transfer (upper chart, black line), apparent heat transfer (upper chart, red line), and energy absorbed by para-ortho H_2 conversion (upper chart, green area) for experiments 1-3. (For interpretation of the references to color in this figure legend, the reader is referred to the web version of this article.)

Fig. 18 summarizes the first full-scale (151 L) para-ortho H_2 experiment performed in a cryogenic pressure vessel (experiments 1-3 in Table 1). The vessel was filled with saturated LH₂

to 68 g/L (10.2 kg, 95% full) and was monitored during pressurization. After 8.5 days of dormancy, the vessel reached 345 bar, with virtually no para-ortho H₂ conversion. Venting 1.2 kg H₂ reduced density to 60 g/L and depressurized the vessel to 210 bar. Active para-ortho H₂ conversion was then observed, starting on day 12 and becoming most active at day 18. Conversion was essentially complete by day 27. Measurement of the green area in the upper chart of Figure 15 revealed that para-ortho H₂ conversion absorbed 35 Watt-days (3 MJ), sufficient to extend dormancy by 7 days at the observed baseline heat transfer rate.

Figures 19-21 show three experiments (5, 7 and 9) conducted at similar H₂ density (~51.4 g/L). Comparing the experimental pressure (green line) and the predicted pressure in the absence of para-ortho H₂ conversion (black dashed line), we can observe that the rate of pressure rise decreases substantially as para-ortho H₂ conversion proceeds, and then increases as para-ortho conversion nears completion. Overall, para-ortho H₂ conversion extends dormancy by about 5 days. The figures show that ortho-H₂ Raman spectroscopy measurements (red circles) are in good agreement with calorimetry (red dashed line). Figures 20 and 21 show that rapid para-ortho H₂ conversion in days 16-18 considerably reduces apparent heat transfer to 1.5 W from a baseline average of 5 W. Minimum apparent heat transfer was higher (2.5 Watts) for experiment 5 (Figure 19) due to higher pressure in the vacuum space leading to higher baseline heat transfer.

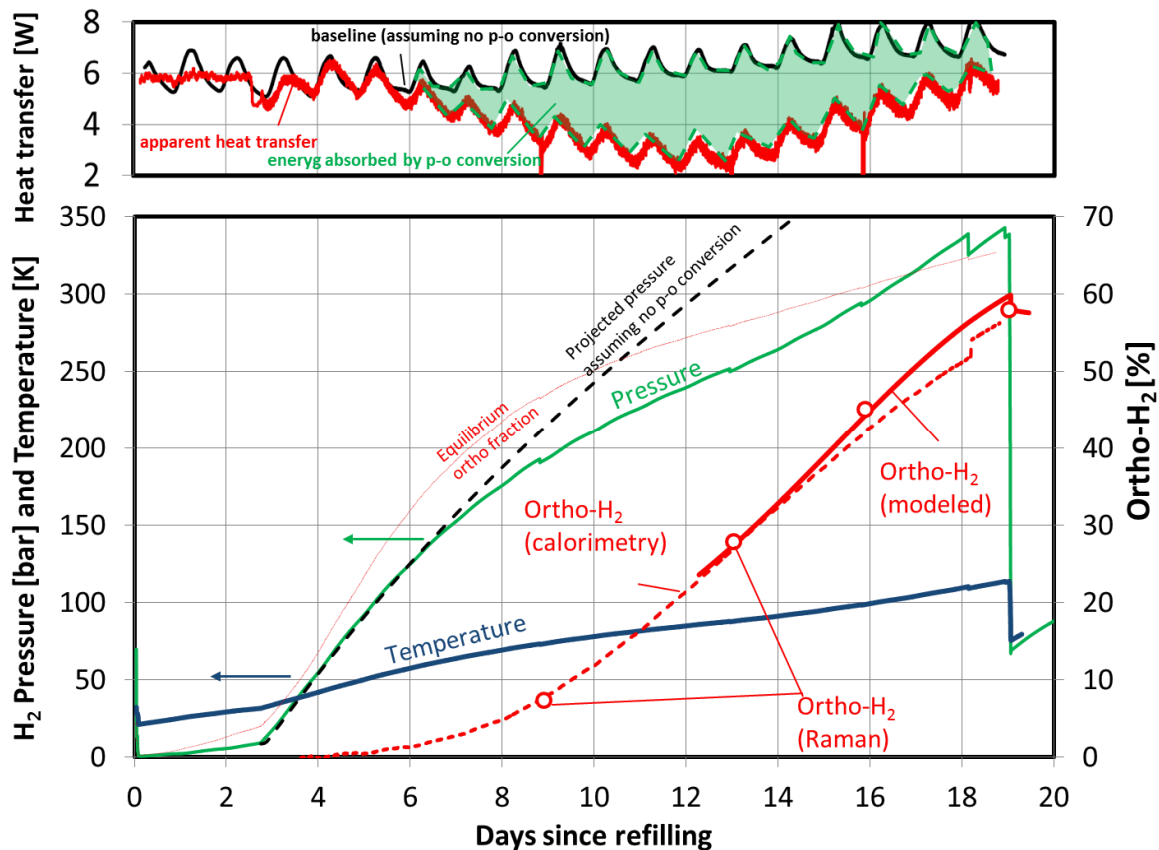


Figure 19. H₂ pressure (green line), pressurization rate with no para-ortho H₂ conversion (black dashed line), temperature (blue line), equilibrium ortho-H₂ fraction (red thin line), measured ortho-H₂ fraction from Raman spectroscopy (red circles), measured ortho-H₂ fraction from calorimetry (red dashed line), modeled ortho-H₂ fraction (thick red line), and baseline heat transfer (upper chart, black line), apparent heat transfer (upper chart, red line), and energy

absorbed by para-ortho H₂ conversion (upper chart, green area) for experiment 5 at density 51.4 gH₂/L. (For interpretation of the references to color in this figure legend, the reader is referred to the web version of this article.)

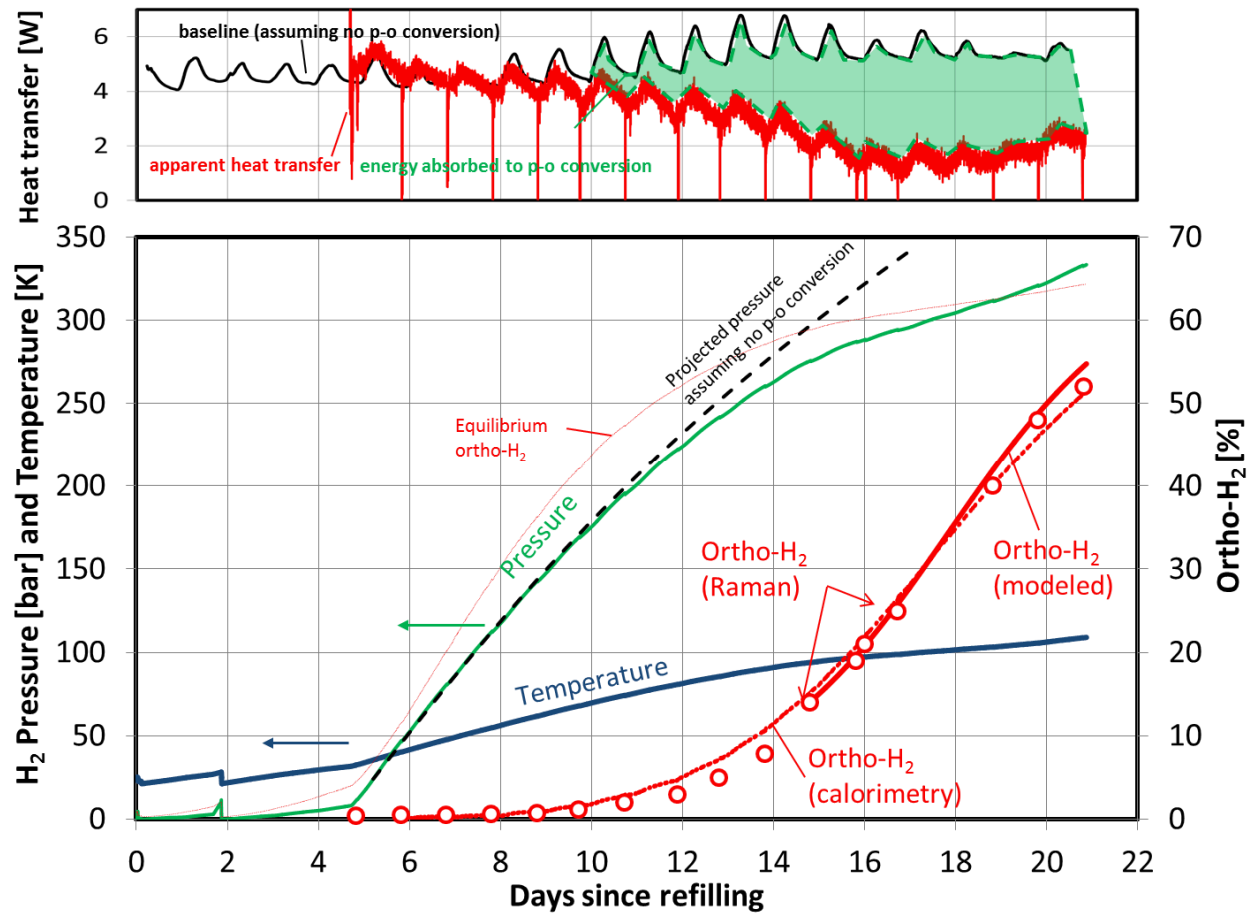


Figure 20. H₂ pressure (green line), pressurization rate with no para-ortho H₂ conversion (black dashed line), temperature (blue line), equilibrium ortho-H₂ fraction (red thin line), measured ortho-H₂ fraction from Raman spectroscopy (red circles), measured ortho-H₂ fraction from calorimetry (red dashed line), modeled ortho-H₂ fraction (thick red line), and baseline heat transfer (upper chart, black line), apparent heat transfer (upper chart, red line), and energy absorbed by para-ortho H₂ conversion (upper chart, green area) for experiment 7 at density 51.4 gH₂/L. (For interpretation of the references to color in this figure legend, the reader is referred to the web version of this article.)

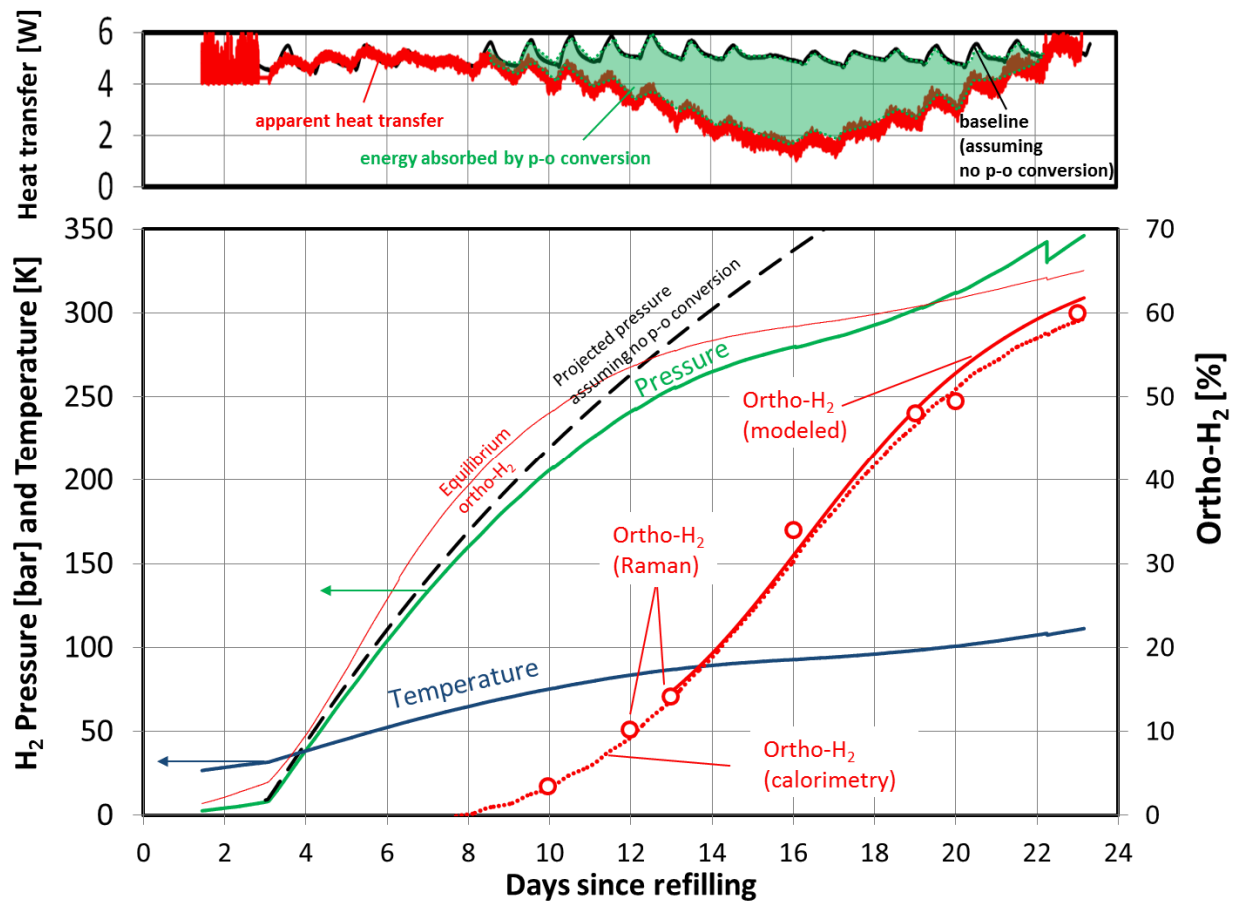


Figure 21. H₂ pressure (green line), pressurization rate with no para-ortho H₂ conversion (black dashed line), temperature (blue line), equilibrium ortho-H₂ fraction (red thin line), measured ortho-H₂ fraction from Raman spectroscopy (red circles), measured ortho-H₂ fraction from calorimetry (red dashed line), modeled ortho-H₂ fraction (thick red line), and baseline heat transfer (upper chart, black line), apparent heat transfer (upper chart, red line), and energy absorbed by para-ortho H₂ conversion (upper chart, green area) for experiment 9 at density 51.3 gH₂/L. (For interpretation of the references to color in this figure legend, the reader is referred to the web version of this article.)

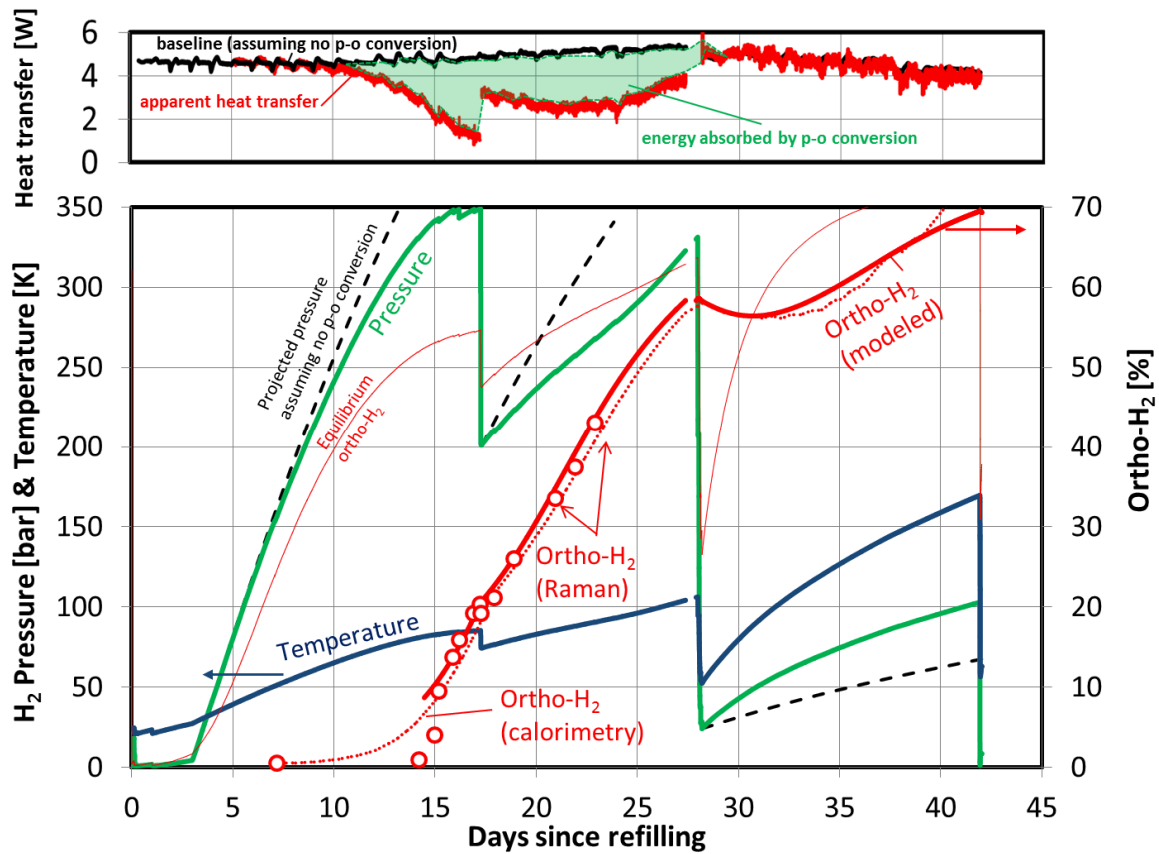


Figure 22. H₂ pressure (green line), pressurization rate with no para-ortho H₂ conversion (black dashed line), temperature (blue line), equilibrium ortho-H₂ fraction (red thin line), measured ortho-H₂ fraction from Raman spectroscopy (red circles), measured ortho-H₂ fraction from calorimetry (red dashed line), modeled ortho-H₂ fraction (thick red line), and baseline heat transfer (upper chart, black line), apparent heat transfer (upper chart, red line), and energy absorbed by para-ortho H₂ conversion (upper chart, green area) for experiments 11-13 with 61.2, 51.8 and 13.8 g/L H₂ densities. (For interpretation of the references to color in this figure legend, the reader is referred to the web version of this article.)

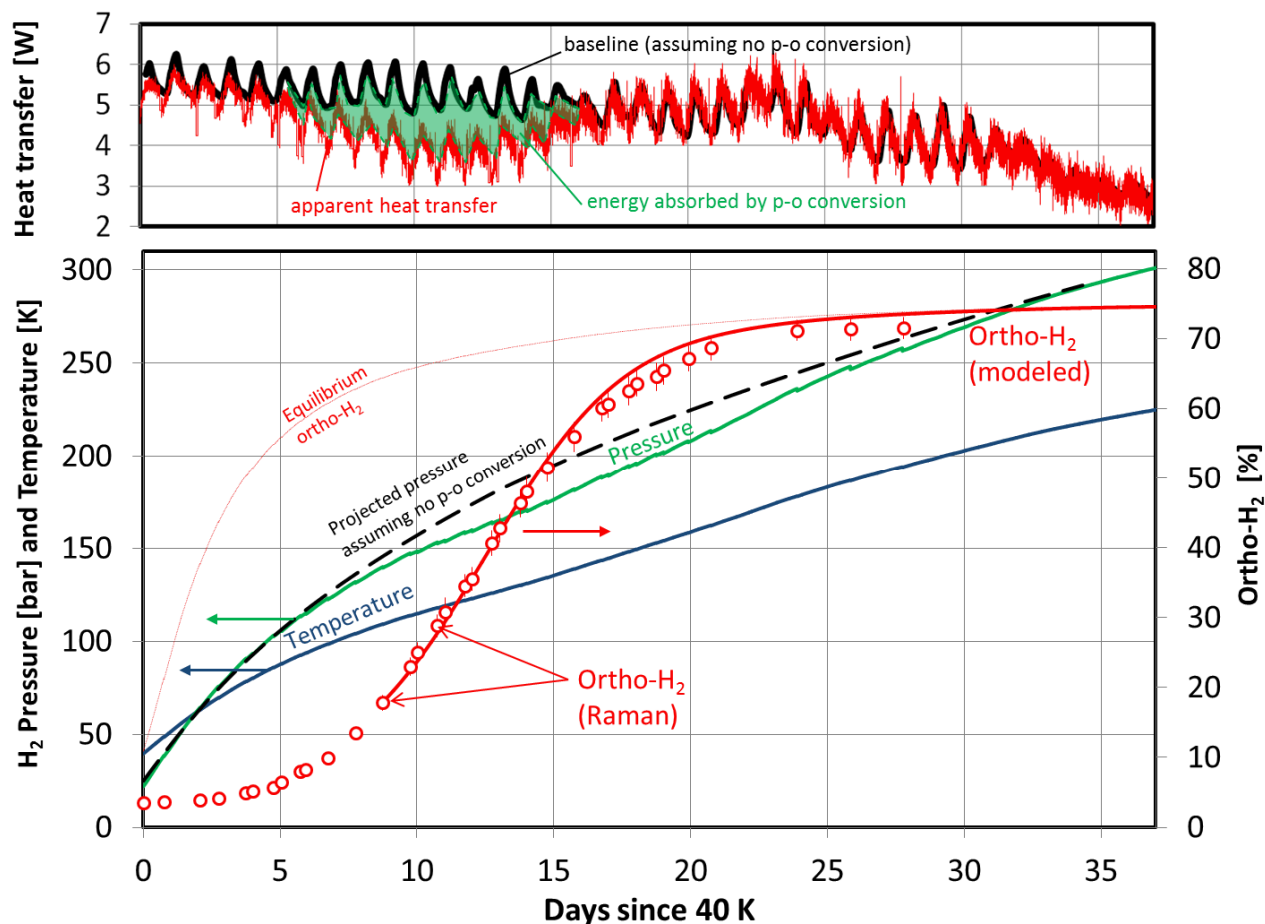


Figure 23. H₂ pressure (green line), pressurization rate with no para-ortho H₂ conversion (black dashed line), temperature (blue line), equilibrium ortho-H₂ fraction (red thin line), measured ortho-H₂ fraction (Raman spectroscopy, red circles), modeled ortho-H₂ fraction (thick red line), and baseline heat transfer (upper chart, black line), apparent heat transfer (upper chart, red line), and energy absorbed by para-ortho H₂ conversion (upper chart, green area) for experiment 15 at density 28 gH₂/L. (For interpretation of the references to color in this figure legend, the reader is referred to the web version of this article.)

Fig. 22 shows experiments 11, 12 and 13 (61.2, 51.8 and 13.8 g/L H₂ densities), where we attempted to study the conversion kinetics at similar density as previous experiments (~51 g/L, experiments 5, 7 and 9) but with different initial temperature (75 K) and ortho-H₂ fraction (19.2% vs. ~3% for experiments 5, 7 and 9 when the temperature equals 75 K). Higher ortho-H₂ fraction in experiment 12 results in doubling of the conversion kinetics (2.5% per day vs. 1.2% per day in experiments 5, 7 and 9). We also observe that some conversion occurred at the high density of experiment 11, lengthening dormancy by ~3 days (days 13-16).

Fig. 23 shows para-ortho H₂ conversion at a low H₂ density of 28 g/L. This lower density enabled full para-ortho H₂ conversion without the need for H₂ venting. We can observe that conversion time (~20 days) is similar to that observed for ~51 gH₂/L (Figures 19-21), although conversion is complete at a much higher temperature (~150 K vs. ~110 K for experiment 9). Para-ortho H₂ cooling (green area in upper chart) is also smaller due to lower H₂ density: the minimum apparent heat transfer is 3.8 Watts for experiment 15 vs. 1.5 Watts for experiment 9.

Fig. 24 emphasizes dormancy gain due to para-ortho H₂ conversion for the high-density experiments (51.3-62.4 gH₂/L). This is the density range of most interest because (1) extended parking is most likely to lead to H₂ venting, and (2) para-ortho H₂ conversion produces the most cooling due to high density. For each experimental line (blue, experiment 14; green, experiment 11; gray, experiment 7; and red, experiment 9) there is a dotted line of the same color indicating the pressurization rate in the absence of para-ortho conversion, i.e. pure para-H₂, so that the dormancy gain of the spin conversion can be directly estimated. For our operating conditions (internal volume of 151 L, rated pressure of 345 bar, ~5 Watts heat transfer), the dormancy gain due to para-ortho conversion is estimated to be about 3 days for experiments 11 and 14 (densities of 61.2 and 62.4 g/L) and 5 days for experiments 7 and 9 (51.3 and 51.4 g/L). Here again, the figure shows that conversion times are similar for the different densities: it takes about 9 to 10 days to convert from 2% to 50% ortho-H₂.

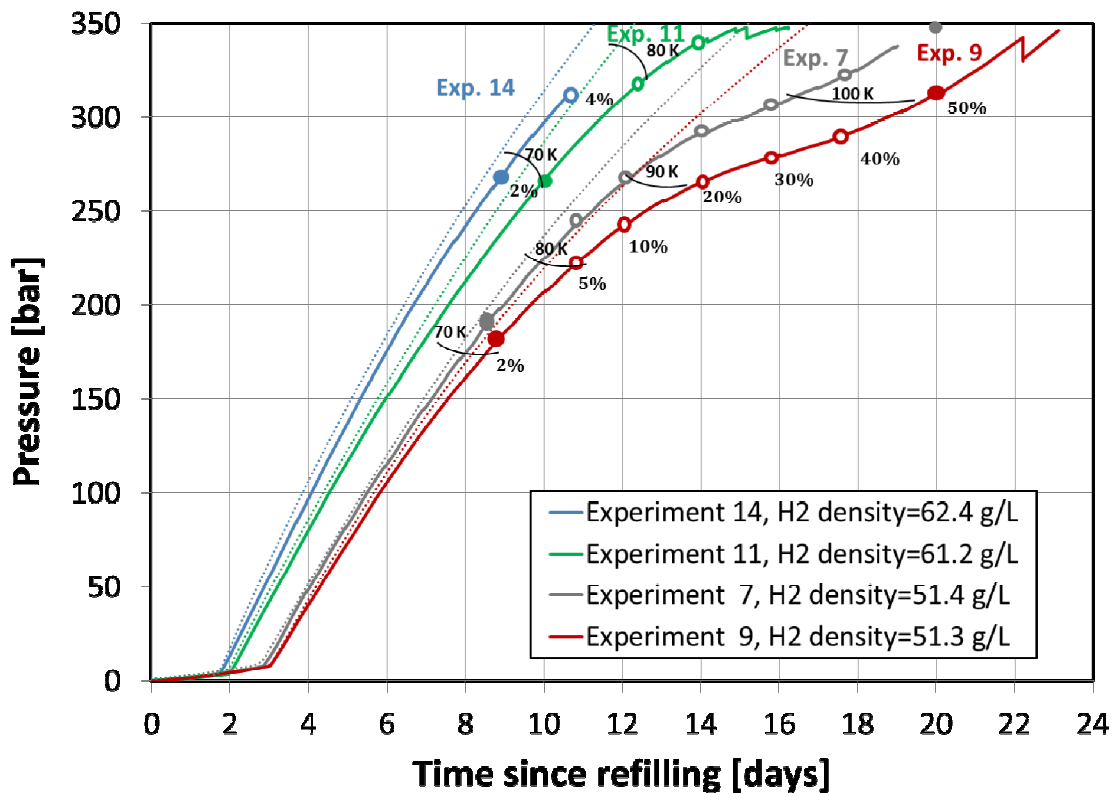


Figure 24. Pressure as a function of time for experiments 7, 9, 11 and 14. The solid lines represent experimental temperatures, and dotted lines are (modeled) pressurization rates in the absence of para-ortho H₂ conversion. Circles represent the ortho-H₂ fraction, in %, for each test. Temperatures are also shown. (For interpretation of the references to color in this figure legend, the reader is referred to the web version of this article.)

8. Conclusions

In a year-long project, we have conducted fifteen para-ortho H₂ conversion experiments in a full-scale 151 liter vessel rated for 345 bar at densities from 14 to 67 g/L. In these experiments, the vessel is initially filled with saturated LH₂ at near ambient pressure (2-3 bar), very cold temperature (20.3-25 K), varying densities, and very high para-H₂ fraction (99.7%). The vessel is subsequently left to pressurize and warm up due to environmental heat transfer. As the vessel warms up, para-H₂ converts to ortho-H₂, absorbing energy and reducing the pressurization and fuel vent rate. Ortho fraction is measured by two approaches: rotational Raman spectroscopy and calorimetry. Experimental results are then compared to an existing para-ortho H₂ kinetic correlation by Milenko et al. [22]. The main results from the project are:

- Experiments show that para-ortho H₂ conversion typically becomes active after 10-15 days of parking, when H₂ temperature reaches 70-80 K. Para-ortho H₂ conversion approaches completion (equilibrium) after 25-30 days when the vessel reaches 100-120 K at ~50 g/L density. Warmer temperatures are necessary for conversion at lower densities, but the number of days remains unchanged.
- Good agreement was observed between ortho-H₂ measurements obtained from rotational Raman spectroscopy and calorimetry. Raman spectroscopy is, however, considered more accurate due to uncertainties in environmental heat transfer rate.
- Vessel rated pressure sets a limit to the maximum density that can be used in para-ortho H₂ conversion experiments. Considering that para-ortho H₂ conversion typically approaches completion at 100-120 K, density is limited to 48-54 g/L within the 345 bar vessel limit. This is confirmed by experiments with 60+ g/L where only partial conversion was achieved before venting became necessary.
- Para-ortho H₂ conversion increases dormancy (time that the vessel can absorb heat from the environment before having to vent fuel to avoid exceeding vessel rating) between 3 and 7 days for the conditions studied here. Considering that the vessel average heat transfer rate is ~5 Watts, para-ortho H₂ conversion cooling equals 15-35 Watt-days (1.3-3 MJ).
- Milenko's kinetic correlation consistently underpredicts para-ortho H₂ conversion rate at the initial low ortho-H₂ fraction and low temperature conditions. This may be partly due to catalytically enhanced conversion at the vessel wall that may play a significant role when ortho-H₂ concentration is below 1%.
- The quality of agreement between experiments and Milenko's correlation consistently improves as the temperature and initial ortho-H₂ fraction increase. We have established ranges of applicability where the correlation and experiments agree to within a coefficient of determination $R^2 > 0.99$.
- The experiments show that the slight decrease of our measured kinetic constants with increasing temperature is consistent with Wigner's original theory [21], although Wigner's original theory predicts different orders of magnitude than the rates we observed. This might suggest that the collision approach distance dependence on temperature may in fact be somewhat weak, a possibility that may be borne out of more precise calculations of paramagnetic molecular collisions in a dense fluid..

Our experimental effort was limited to ~50 g/L H₂ density due to the vessel rating (345 bar). Higher pressure cryogenic vessels are now planned that may enable higher density para-ortho H₂ conversion experiments. Ultimately, a controlled temperature apparatus is necessary to fully

research para-ortho H₂ kinetics over the entire range of pressures and temperatures of interest for cryogenic hydrogen storage.

Acknowledgments

The authors kindly acknowledge Diane Cooke (presently at GE Power & Water) for her assistance in performing Raman measurements; Timothy O. Ross and Vern A. Switzer (LLNL) for conducting the H₂ refueling, monitoring and sampling; and the BMW AG's Hydrogen Storage Department for valuable discussions during experimental design and results analysis. This project was funded by DOE, Office of Fuel Cell Technologies, Ned Stetson and Erika Sutherland, Technology Development Managers. This work performed under the auspices of the U.S. Department of Energy by Lawrence Livermore National Laboratory under Contract DE-AC52-07NA27344.

References

- [1] Bowman B, Klebanoff LE. Historical Perspectives on Hydrogen, its Storage and Applications. Hydrogen Storage Technology, Materials and Applications, Boca Raton: Taylor & Francis; 2012, p. 65.
- [2] Aceves SM, Martinez-Frias J, Garcia-Villazana O. Analytical and experimental evaluation of insulated pressure vessels for cryogenic hydrogen storage. *International Journal of Hydrogen Energy* 2000;25:1075–85.
- [3] Aceves SM, Berry GD, Martinez-Frias J, Espinosa-Loza F. Vehicular storage of hydrogen in insulated pressure vessels. *International Journal of Hydrogen Energy* 2006;31:2274–83.
- [4] Aceves SM, Espinosa-Loza F, Ledesma-Orozco E, Ross TO, Weisberg AH, Brunner TC, et al. High-density automotive hydrogen storage with cryogenic capable pressure vessels. *International Journal of Hydrogen Energy* 2010;35:1219–26.
- [5] Aceves SM, Petitpas G, Espinosa-Loza F, Matthews MJ, Ledesma-Orozco E. Safe, long range, inexpensive and rapidly refuelable hydrogen vehicles with cryogenic pressure vessels. *International Journal of Hydrogen Energy* 2013;38:2480–9.
- [6] Wallner T, Lohse-Busch H, Gurski S, Duoba M, Thiel W, Martin D, et al. Fuel economy and emissions evaluation of BMW Hydrogen 7 Mono-Fuel demonstration vehicles. *International Journal of Hydrogen Energy* 2008;33:7607–18.
- [7] Pauling L, Jr EBW, Physics. Introduction to Quantum Mechanics with Applications to Chemistry. Dover Publications; 1985.
- [8] Souers PC. Hydrogen Properties for Fusion Energy. Univ of California Pr; 1986.
- [9] Reif F. Fundamentals of statistical and thermal physics. Long Grove, Ill.: Waveland Press; 2009.
- [10] Flynn TM. Cryogenic Engineering, Second Edition, Revised and Expanded. 2nd ed. CRC Press; 2004.
- [11] Shevtsov V, Scherbakov A, Malmi P, Ylinen E, Punkkinen M. Ortho-para conversion in solid hydrogen, catalyzed by molecular oxygen impurities. *Journal of Low Temperature Physics* 1996;104:211–35.
- [12] Andrews L, Wang X. A discharge investigation of hydrogen and deuterium atom formation, and parahydrogen and orthodeuterium reconversion. *The Journal of Chemical Physics* 2004;121:4724–9.

- [13] Golden S, Peiser AM, Katz S. The thermal ortho-para conversion of hydrogen. New-York: Office of Naval Research; 1952.
- [14] Emmett PH, Harkness RW. The conversion of para hydrogen to ortho hydrogen over iron synthetic ammonia catalysts. *J Am Chem Soc* 1932;54:403–4.
- [15] West W. The Use of the Ortho—Para Hydrogen Conversion in the Detection of Free Radicals Produced in Photo-dissociation1. *J Am Chem Soc* 1935;57:1931–4.
- [16] Farkas A. Orthohydrogen, Parahydrogen and Heavy Hydrogen. The Cambridge Series of Physical Chemistry; 1935.
- [17] McCarthy RD. Hydrogen: its technology and implications. CRC Press; 1975.
- [18] Bose T, Malbrunot P. Hydrogen: Facing the Energy Challenges of the 21st Century. John Libbey Eurotext; 2007.
- [19] Baker CR, Shaner RL. A study of the efficiency of hydrogen liquefaction. *International Journal of Hydrogen Energy* 1978;3:321–34.
- [20] Cremer E, Polyani M. The conversion of o- to p-hydrogen in solid state. *Zeitschrift Fur Physikalische Chemie* 1933;B21:459–68.
- [21] Wigner E. Concerning the paramagnetic conversion of para-ortho hydrogen III (in german). *Zeitschrift Fur Physikalische Chemie* 1933;B23.
- [22] Milenko YY, Sibileva RM, Strzhemechny MA. Natural ortho-para conversion rate in liquid and gaseous hydrogen. *J Low Temp Phys* 1997;107:77–92.
- [23] Matthews MJ, Petitpas G, Aceves SM. A study of spin isomer conversion kinetics in supercritical fluid hydrogen for cryogenic fuel storage technologies. *Applied Physics Letters* 2011;99:081906.
- [24] Lemmon EW, Huber ML, McLinden MO. NIST Standard Reference Database 23: Reference Fluid Thermodynamic and Transport Properties-REFPROP 2007.
- [25] Peng JK, Ahluwalia RK. Enhanced dormancy due to para-to-ortho hydrogen conversion in insulated cryogenic pressure vessels for automotive applications. *International Journal of Hydrogen Energy* 2013;38:13664–72.
- [26] Younglove BA. Thermophysical Properties of Fluids: Argon, Ethylene, Parahydrogen, Nitrogen, Nitrogen Trifluoride, and Oxygen. American Institute of Physics; 1982.